Cell Reports
Medicine

Article

RNF31 inhibition sensitizes tumors to bystander killing by innate and adaptive immune cells

Graphical abstract

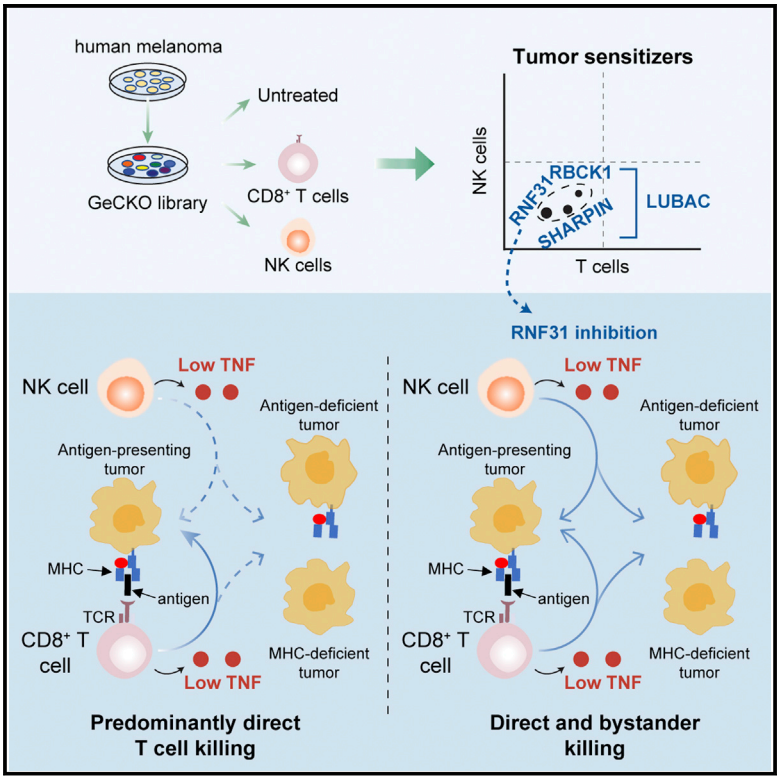

Highlights

- Parallel CRISPR screens in tumor cells identify NK and T cell susceptibility genes
- Ablation of LUBAC ubiquitination complex sensitizes tumors to immune elimination
- Small-molecule RNF31 inhibition sensitizes tumor cells in TNF-dependent fashion
- RNF31 inhibition strongly enhances immune bystander killing

Authors

Zhengkui Zhang, Xiangjun Kong, Maarten A. Ligtenberg, ..., Sjoerd Klarenbeek, Maarten Altelaar, Daniel S. Peeper

Correspondence

d.peeper@nki.nl

In brief

Zhang et al. identify by CRISPR-Cas9 knockout screening in tumor cells all components of the LUBAC linear ubiquitination complex: RNF31, SHARPIN, and RBCK1. Genetic or pharmacologic inhibition of RNF31 sensitizes tumors to both NK and CD8+ T cell killing by disrupting TNF receptor complex I signaling, while enhancing bystander killing.

Zhang et al., 2022, Cell Reports Medicine 3, 100655
June 21, 2022
https://doi.org/10.1016/j.xcrm.2022.100655

CellPress

Cell Reports Medicine

CellPress
OPEN ACCESS

Article

RNF31 inhibition sensitizes tumors to bystander killing by innate and adaptive immune cells

Zhengkui Zhang,[1,8] Xiangjun Kong,[1,5,8] Maarten A. Ligtenberg,[1,6,8] Susan E. van Hal-van Veen,[1] Nils L. Visser,[1] Beaunelle de Bruijn,[1,7] Kelly Stecker,[4] Pim W. van der Helm,[1] Thomas Kuilman,[1,5] Esmée P. Hoefsmit,[1] David W. Vredevoogd,[1] Georgi Apriamashvili,[1] Beau Baars,[1] Emile E. Voest,[1] Sjoerd Klarenbeek,[3] Maarten Altelaar,[2,4] and Daniel S. Peeper[1,9,*]

[1]Division of Molecular Oncology and Immunology, Oncode Institute, the Netherlands Cancer Institute, Plesmanlaan 121, 1066 CX Amsterdam, the Netherlands
[2]Proteomics Core Facility, the Netherlands Cancer Institute, Plesmanlaan 121, 1066 CX Amsterdam, the Netherlands
[3]Experimental Animal Pathology, the Netherlands Cancer Institute, Plesmanlaan 121, 1066 CX Amsterdam, the Netherlands
[4]Biomolecular Mass Spectrometry and Proteomics, Bijvoet Center for Biomolecular Research and Utrecht Institute for Pharmaceutical Sciences, University of Utrecht, and Netherlands Proteomics Center, Padualaan 8, 3584 CH Utrecht, the Netherlands
[5]Present address: Neogene Therapeutics, Amsterdam, the Netherlands
[6]Present address: Immagene, Oss, the Netherlands
[7]Present address: Laboratory for Intravital Imaging and Dynamics of Tumor Progression, VIB Center for Cancer Biology, Department of Oncology, KU Leuven, Leuven, Belgium
[8]These authors contributed equally
[9]Lead contact
*Correspondence: d.peeper@nki.nl
https://doi.org/10.1016/j.xcrm.2022.100655

SUMMARY

Tumor escape mechanisms for immunotherapy include deficiencies in antigen presentation, diminishing adaptive CD8$^+$ T cell antitumor activity. Although innate natural killer (NK) cells are triggered by loss of MHC class I, their response is often inadequate. To increase tumor susceptibility to both innate and adaptive immune elimination, we performed parallel genome-wide CRISPR-Cas9 knockout screens under NK and CD8$^+$ T cell pressure. We identify all components, RNF31, RBCK1, and SHARPIN, of the linear ubiquitination chain assembly complex (LUBAC). Genetic and pharmacologic ablation of RNF31, an E3 ubiquitin ligase, strongly sensitizes cancer cells to NK and CD8$^+$ T cell killing. This occurs in a tumor necrosis factor (TNF)-dependent manner, causing loss of A20 and non-canonical IKK complexes from TNF receptor complex I. A small-molecule RNF31 inhibitor sensitizes colon carcinoma organoids to TNF and greatly enhances bystander killing of MHC antigen-deficient tumor cells. These results merit exploration of RNF31 inhibition as a clinical pharmacological opportunity for immunotherapy-refractory cancers.

INTRODUCTION

Immunotherapy has dramatically revolutionized the care of cancer patients, most profoundly those suffering from melanoma. Immune checkpoint blockade (ICB) and adoptive T cell transfer therapies serve to (re-)invigorate tumor-specific CD8$^+$ T cell function.[1,2] However, for melanoma, but more frequently for other cancer indications, either primary or acquired resistance limits overall and durable patient benefit.[3] Among the mechanisms driving upfront resistance are those related to the inability of tumor cells to present (neo-)antigens to CD8$^+$ T cells. Deficiencies in this antigen presentation machinery prevent cytotoxic T cells from recognizing their targets and hence contribute to both tumorigenesis and immunotherapy resistance.[4] For example, mutations in proteasome subunits, transporters, beta-2-microglobulin (B2M) (required for MHC class I folding and stable cell surface localization), and MHC class I itself all contribute to T cell surveillance escape[5–9] and are observed in up to 78% of lung cancers.[10,11]

These limitations of CD8$^+$ T cell antitumor activity may be tackled in part by the innate immune system. Natural killer (NK) cells are innate immune cells that can directly eliminate tumor cells independent of TCR-MHC class I/antigen interactions. However, much like T cells, upon encountering tumors NK cells can get activated and release cytotoxic particles containing granzymes as well as cytokines, including interferon gamma (IFN-γ), tumor necrosis factor (TNF), and Fas ligand.[12,13] In this way, NK cells cannot only trigger caspase-dependent death in tumors,[14,15] but also enhance adaptive immunity.[16] However, this is not a watertight line of defense, given the common emergence of cancers in many (immunotherapy-treated) patients. The degree of NK cell activation is determined by a complex array of signals.[16,17] On the tumor side, loss of MHC class I expression relieves intrinsic NK cell inhibition. However, the net activity of NK cells is influenced by several additional factors, including

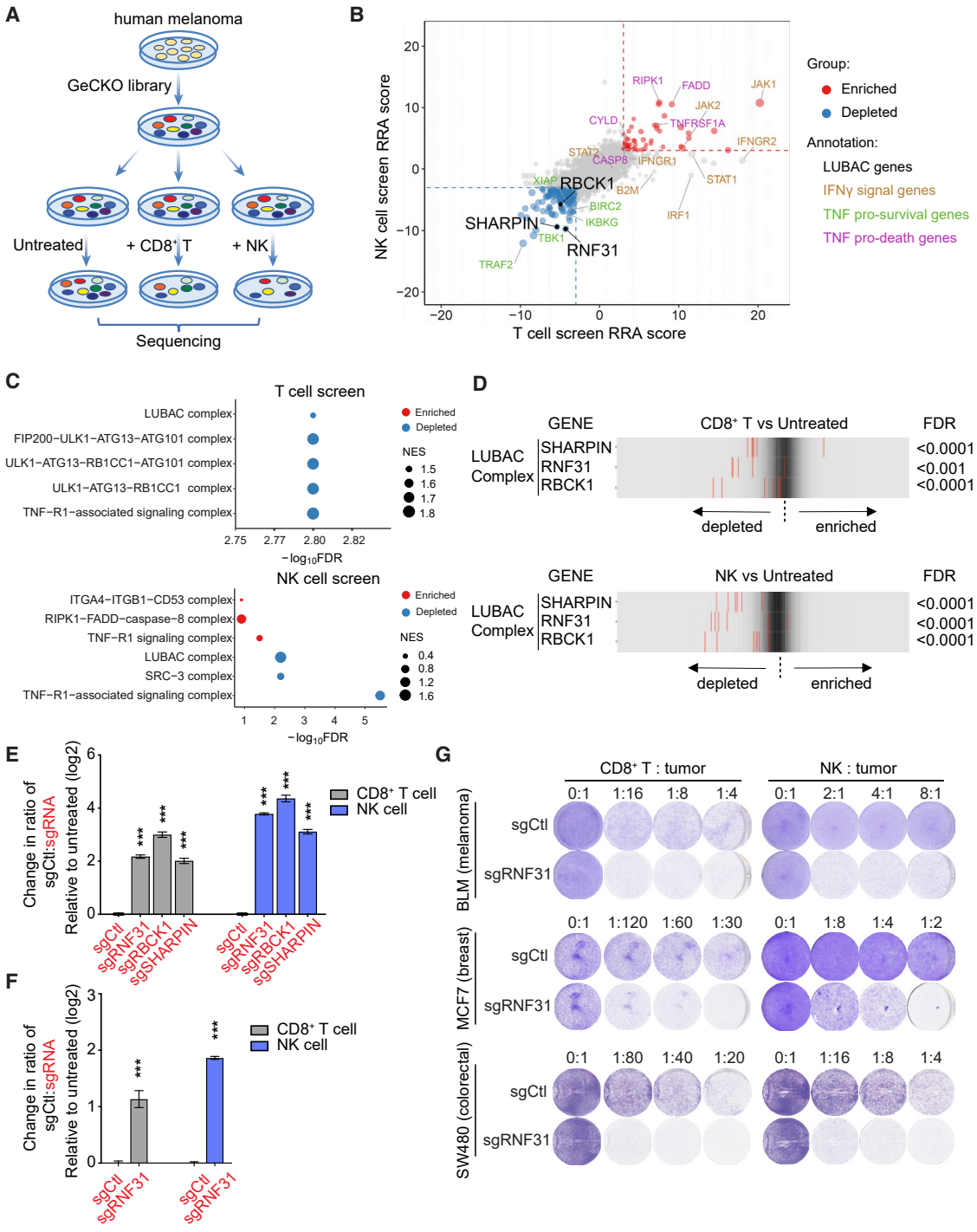

Figure 1. Genome-wide CRISPR-Cas9 library screens identify all LUBAC components that protect tumor cells against CD8+ T and NK cell killing

(A) Schematic overview of parallel CRISPR-Cas9 knockout screens in D10 human melanoma cells upon challenge with either CD8+ T cells or NK cells.

(B) Robust ranking aggregation (RRA) plot showing top enriched genes (red) or depleted genes (blue) from both CD8+ T and NK cell screen arms. –Log10 transformed MAGeCK RRA scores were used. Dashed line indicates –Log10 transformed RRA score at 3 or –3. Dot sizes are scaled by Log2 fold change. Annotated genes represent LUBAC (black), IFN-γ signaling (brown), TNF prosurvival signaling (green), and TNF pro-death signaling (purple) genes.

(C) Gene set enrichment analysis (GSEA) of significantly enriched genes (red) or depleted genes (blue) in CD8+ T or NK cell screen using MAGeCKFlute. Parts of enriched complexes are plotted. The p values were calculated based on the hypergeometric distribution. The size of each circle indicates normalized enrichment scores (NES) that are enriched in the corresponding function.

(legend continued on next page)

inhibiting and activating surface molecules.[18] Moreover, the degree of tumor infiltration with NK cells,[19,20] and cytotoxic T cells for that matter, represents an important factor determining immune antitumor activity.[16,21–23]

To uncover not only new therapeutic targets for immuno-oncology but also address the problem of immune escape involving CD8$^+$ T and NK cells, here we set out to perform parallel genome-wide CRISPR-Cas9 knockout screens, aiming to find tumor-intrinsic sensitizers to both MHC class I- and antigen-dependent CD8$^+$ T cell killing and MHC- and antigen-independent NK cell killing. Furthermore, upon validating several hits common to both screen settings, we studied how innate and adaptive immunity contribute to antitumor activity. Finally, as a translational outlook, we investigated whether genetic ablation of our top hit could be recapitulated with a small-molecule approach.

RESULTS

Genome-wide CRISPR-Cas9 library screens identify all LUBAC components that protect tumor cells against CD8$^+$ T and NK cell killing

To genetically identify genes modulating both CD8$^+$ T (MHC- and antigen-dependent) and NK (MHC- and antigen-independent) killing of tumor cells, we performed parallel genome-wide CRISPR-Cas9 knockout screens in human melanoma cells after either CD8$^+$ T cell or NK cell challenge. To study interactions between tumor cells and CD8$^+$ T cells, we previously established a matched human tumor:T cell co-culture system.[24] Specifically, D10 melanoma cells, which endogenously express HLA-A*02:01/MART-1, were challenged with healthy donor CD8 T cells retrovirally transduced with a MART-1-specific T cell receptor (MART-1 CD8$^+$ T cells).[25,26] To study tumor susceptibility to NK elimination, we used KHYG-1, a human NK cell line with high cytotoxicity against tumor cells.[27–29] With these systems, we performed two parallel unbiased genome-wide CRISPR-Cas9 knockout screens (Figure 1A). Tumor cells were infected in duplicate with the GeCKO library[30] at 1,000× coverage and then challenged with either MART-1 CD8$^+$ T cells or NK cells. The selection pressure for the screens was optimized such that both immune resistance and sensitization genes would be uncovered. The surviving cells were harvested, and single-guide RNAs (sgRNAs) were subsequently recovered by PCR amplification of genomic DNA and analyzed by deep sequencing to identify sgRNAs that were either enriched (causing immune resistance) or depleted (causing immune sensitization; Table S1).

In the CD8$^+$ T cell-treated screen arm, we identified genes involved in the IFN-γ pathway, antigen presentation, autophagy, and the TNF pathway, which was expected because of their established roles in T cell-mediated killing[24,31–36] (Figures S1A and S1B). In contrast, in the NK cell-treated screen arm, IFNGR2, JAK2, STAT1, and IRF1, which constitute critical components of the IFN-γ pathway and stimulate MHC class I expression, were not enriched (Figures S1A and S1B). Taken together, the result confirmed the screen specificity for CD8$^+$ T cell- and NK cell-mediated killing.

Given the focus on common immune escape mechanisms in this study, we were interested to uncover genes whose ablation increased susceptibility to elimination by both CD8$^+$ T and NK cells. Indeed, we identified several genes that were either commonly depleted or enriched. In the latter category, we identified a number of genes from the TNF pro-death pathway, including TNFRSF1A, RIPK1, FADD, and CASP8 (Figure 1B, upper right quadrant, Figure S1B). This result is consistent with the idea that deficiencies in TNF-associated pro-death signaling render tumor cells resistant to both CD8$^+$ T cell- and NK cell-mediated antitumor activity.[24,31,34,37] Most interestingly, RNF31, RBCK1, and SHARPIN, all three components of the linear ubiquitin chain assembly complex (LUBAC), dropped out significantly in both CD8$^+$ T and NK cell screens (Figure 1B, lower left quadrant). Gene set enrichment analysis (GSEA) with both positively and negatively selected genes illustrated that LUBAC is one of the top enriched complexes (Figure 1C), which was confirmed by distribution analysis of individual sgRNAs (Figure 1D).

To validate all three LUBAC components, CFSE-labeled melanoma cells transduced with sgRNAs targeting either RNF31, RBCK1, or SHARPIN were admixed 1:1 with CTV-labeled sgCtl-transduced cells and used in CD8$^+$ T cell and NK cell cytotoxicity competition assays. Flow cytometric analysis confirmed that genetic ablation of each of the LUBAC components strongly sensitizes tumor cells to both CD8$^+$ T cell and NK cell killing (Figures 1E and S1C). For the remainder of this study we focused on RNF31, because it is a linear ubiquitin ligase and the executive enzyme of LUBAC, and therefore amenable in principle to pharmacologic interference.

We confirmed the effect of RNF31 depletion in another melanoma cell line (BLM), engineered to ectopically express HLA-A*02:01/MART-1 for CD8$^+$ T cell recognition. RNF31 ablation sensitized tumor cells to both CD8$^+$ T and NK cell killing (Figures 1F and S1D). Then, we expanded the cell line panel to breast (MCF7) and colorectal (SW480) tumor cells. These other tumor cell lines were also highly sensitized to both CD8$^+$ T and NK cell killing upon genetic inactivation of RNF31 (Figures 1G and S1E). Thus, depletion of either of three LUBAC components, including RNF31, strongly sensitizes cells from different tumor indications to both NK and CD8$^+$ T cell killing.

RNF31 loss enhances tumor rejection in immune-proficient mice

We next determined whether RNF31 loss provokes tumor immune clearance *in vivo* in murine B16F10-OVA melanoma and

(D) Distribution of individual sgRNAs targeting the LUBAC complex components in both screens.

(E and F) Competition assays of human melanoma D10 cells (E) or BLM cells (F) expressing indicated sgRNAs and treated with MART-1 CD8$^+$ T cells or NK KHYG-1 cells, respectively, analyzed by flow cytometry. The original flow cytometry plots are shown in Figures S1C and S1D. The change in ratio of sgCtrl versus a sgRNA targeting a hit (red) is represented relative to melanoma cells without immune cell challenge (log2 transformed) (n = 3). Error bars indicate SD. Statistics are calculated by unpaired two-sided Student's t test. ***$p < 0.001$.

(G) Cancer cell lines from various tissue of origin (BLM, SW480, and MCF-7 ectopically expressing HLA-A* A2:01 and MART-1 antigen) expressing RNF31 or control sgRNA challenged with increasing numbers of MART-1 CD8$^+$ T or NK cells. Tumor cells were fixed and stained with crystal violet 4–5 days later.

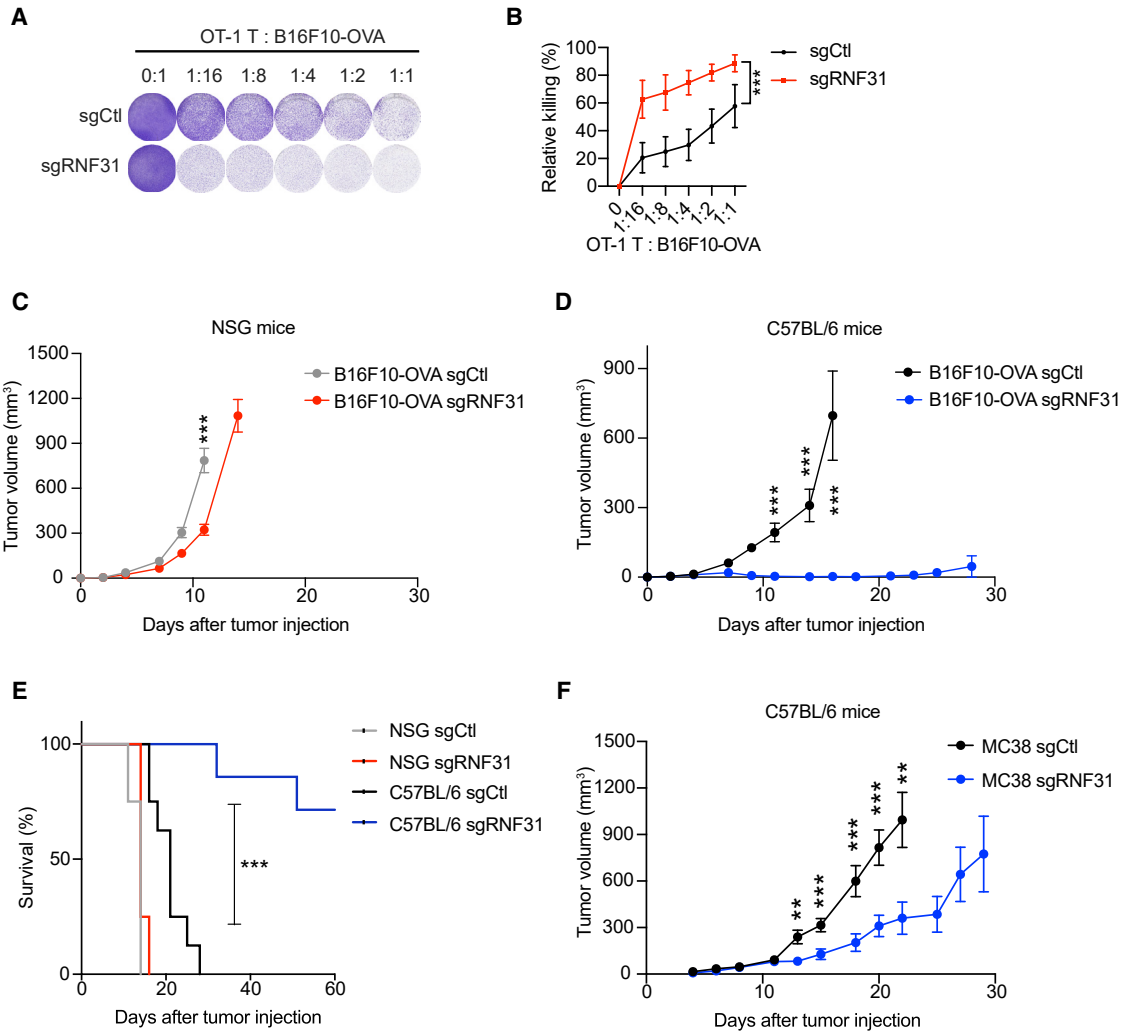

Figure 2. RNF31 loss enhances tumor rejection in immune-proficient mice

(A and B) Mouse melanoma B16F10 cells expressing ovalbumin antigen (OVA) and sgRNF31 or control sgRNA challenged with increasing numbers of OT-1 T cells (A). Cells were fixed and stained with crystal violet 4 days later. Quantification of (A), relative killing is normalized to each untreated group (B). Every T/E ratio shows the average and SD of 3 biological replicates, each with two to three technical replicates. Statistical significance was determined using a two-way ANOVA with Sidak's multiple comparisons test. ***$p < 0.001$.

(C and D) *In vivo* growth of B16F10-OVA cell pools carrying either sgCtl or sgRNF31. Tumor cells were s.c. injected into the flank of either immune-deficient NSG mice (C) or immune-proficient C57BL/6 mice (D). Tumor volume was measured. Error bars indicate SEM; n = 8 mice per group (one mouse was removed from the B16F10-OVA sgRNF31 group in C57BL/6 mice because it showed RNF31 expression in the tumor similar to controls).

(E) Kaplan-Meier survival curves of mice from (C) and (D). Mice were sacrificed after tumors reached 1,000 mm^3. ***$p < 0.001$ by log rank test.

(F) *In vivo* growth of MC38 cell pools carrying either sgCtl or sgRNF31. Tumor cells were s.c. injected into the flank of immune-proficient C57BL/6 mice. Error bars indicate SEM; n = 8 mice per group. (C), (D), and (F) were evaluated by a multiple unpaired two-sided Student's t test. ***$p < 0.001$, **$p < 0.01$.

MC38 colon cancer graft immune-proficient models. First, we confirmed that RNF31 depletion sensitizes also B16F10-OVA cells to OVA-specific OT-1 T cell killing *in vitro* (Figures 2A and 2B). For the B16F10-OVA model, we injected either control sgRNA-transduced or RNF31 knockout B16F10-OVA cell pools into either immune-competent C57BL/6 or immune-deficient NSG mice. RNF31-deficient B16F10-OVA tumors expanded more slowly than control ones in NSG mice (Figures 2C and S2A). A similar trend was observed for human D10 RNF31-deficient melanoma cells, suggesting a requirement of RNF31 for full tumor growth (Figure S2B). However, the effects of RNF31 ablation were more pronounced in immuno-competent C57BL/6 mice, where the RNF31-deficient B16F10-OVA tumors were much more rapidly cleared (5/7) than control tumors (0/8) (Figures 2D and S2C). These results indicate an important contribution of immune pressure for the clearance of RNF31-deficient tumors. As a result, RNF31-deficient tumor-bearing C57BL/6 mice but not NSG mice showed prolonged survival (Figure 2E). RNF31 knockout MC38 tumors also grew much more slowly and (C57BL/6) mice survived significantly longer (Figures 2F,

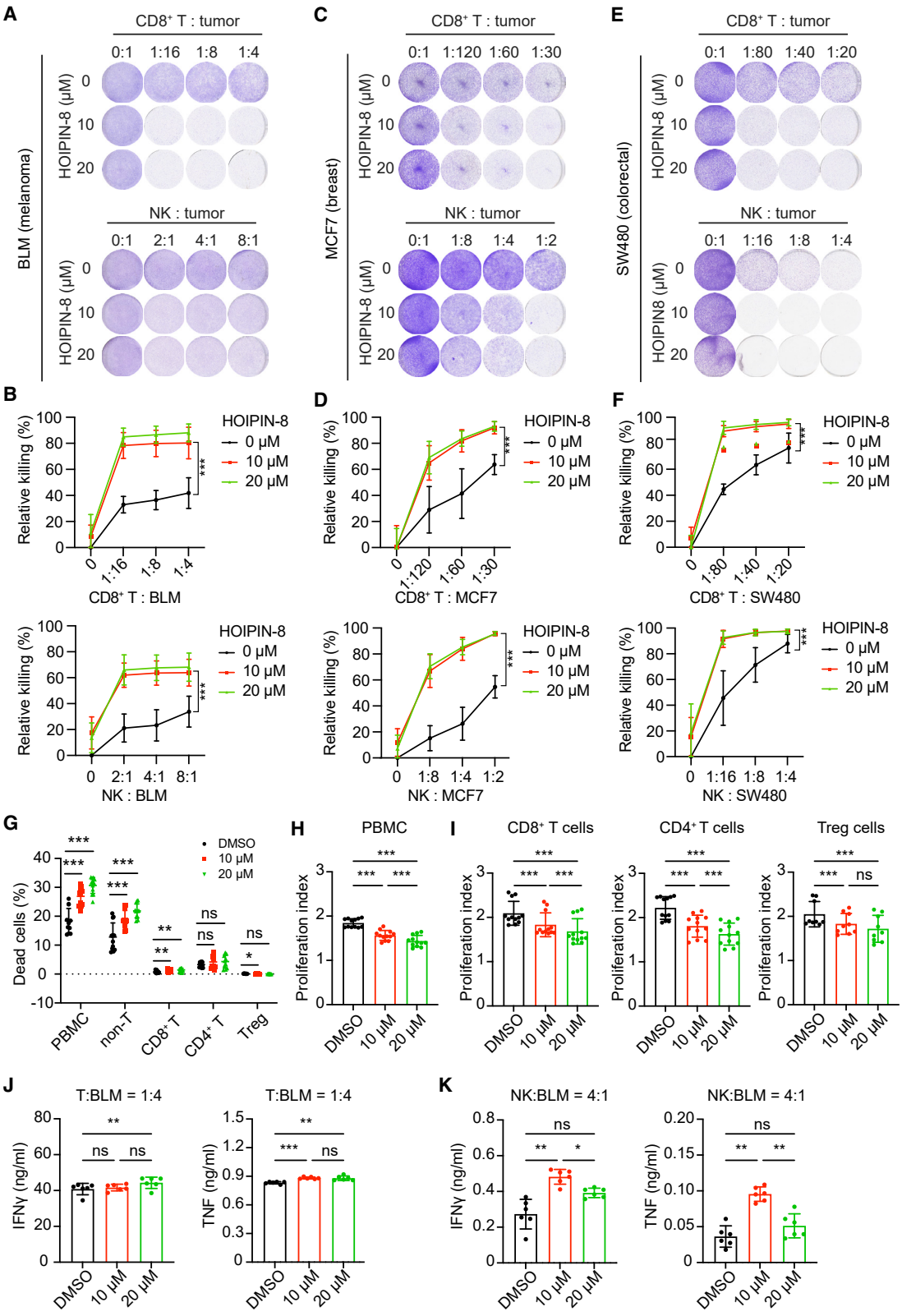

(legend on next page)

S2D, and S2E). RNF31 knockout MC38 tumors showed more infiltration of NK cells but not CD8$^+$ T cells (Figure S2F). These results demonstrate that RNF31 loss triggers strong immune rejection of tumors *in vivo*.

Pharmacologic inhibition of RNF31 enhances tumor sensitivity to both CD8$^+$ T cell- and NK cell-mediated killing

To translate these observations to a preclinical setting, we set out to use a small-molecular inhibitor, HOIPIN-8, to target RNF31. HOIPIN-8 is a recently developed inhibitor, which shows potent suppression of linear ubiquitination activity of LUBAC *in vitro*.[38–40] We used the relatively immune-resistant human BLM melanoma cells[24] to investigate whether HOIPIN-8 can recapitulate the genetic inactivation of RNF31. Whereas treatment with HOIPIN-8 alone did not alter tumor cell viability, upon co-treatment with either CD8$^+$ T or NK cells a clear cooperation was observed for tumor cell killing (Figures 3A and 3B). This strong immune-dependent sensitization effect by HOIPIN-8 treatment was not limited to melanoma but also seen in breast and colorectal cancer cells (Figures 3C–3F). We observed that HOIPIN-8 should exert continuous pressure on the tumor cells, because after a 24 h pre-treatment followed by washout and T cell or NK cell challenge, the sensitization was considerably reduced (Figures S3A and S3B). Together, these data demonstrate that pharmacological inhibition of RNF31 can mimic genetic ablation and greatly augments tumor cell sensitivity to both CD8$^+$ T and NK cell killing.

Given that RNF31 is expressed also in immune cells,[41,42] we investigated any impact of HOIPIN-8 on this compartment. Although HOIPIN-8 treatment triggered considerable cell death in total PBMCs, this was mostly attributed to non-T cells and did not significantly affect the survival of CD8$^+$, CD4$^+$ T cells, and Tregs (Figures 3G and S3C). HOIPIN-8 also suppressed the proliferation of all these immune cells somewhat (Figures 3H, 3I, and S3D–S3G). However, it did not inhibit the secretion of either IFN-γ or TNF from CD8$^+$ T cells or NK cells in a co-culture assay (Figures 3J and 3K). Consistent with previous studies,[42,43] targeting RNF31 caused a significant reduction in Tregs (Figure S3H), but the CD8$^+$ T/Treg ratio was not negatively affected (Figure S3I). Together, these results show that, although HOIPIN-8 has some impact on the immune cell compartment, it did not result in reduced antitumor activity in this co-culture system. The blood concentration of HOIPIN-8 upon intravenous administration is very low, precluding pharmacologic preclinical validation (Figure S3J).

HOIPIN-8 treatment enhances bystander killing of tumor cells deficient in antigen presentation

Accumulating clinical evidence indicates that immune-evaded cancers have often lost antigen expression or harbor deficiencies in their antigen presentation machinery.[44–48] Our findings of RNF31 inhibition-mediated tumor sensitization to immune cell-mediated killing raise the interesting possibility that immune-evaded tumor cells may be eliminated by administering HOIPIN-8 to enhance the antitumor activity of immune cells in the tumor microenvironment, a process called bystander killing.[44,49,50] To test this hypothesis, we mixed antigen-positive B16F10-OVA tumor cells with antigen-negative ones at different ratios, and subsequently challenged them with OT-1 T cells that recognize and kill OVA antigen-expressing cells (Figure 4A). At a 1:1 ratio, in the control vehicle-treated group, as we expected, OT-1 T cells were only able to kill around 50% of cells (Figures 4B and 4C). In contrast, in the HOIPIN-8-treated group, up to 90% of cells were eliminated by OT-1 T cells. Even at a ratio of 1:9 where only 10% of tumor cells could be recognized by OT-1 T cells, treatment with HOIPIN-8 led to elimination of majority of tumor cells (Figures 4B and 4C).

To mimic antigen presentation machinery deficiency resulting in tumor immune evasion also in a different way, we established B2M-knockout B16F10-OVA cells. B2M is an essential component of the MHC class I complex; in its absence there is no MHC class I antigen presentation (Figure S4). Mixing experiments with parental B16F10-OVA cells and B16F10-OVA B2M KO cells had a similar outcome as above: HOIPIN-8 treatment greatly enhanced bystander killing of antigen presentation machinery-deficient tumor cells by OT-1 T cells (Figures 4D–4F). Collectively, with multiple tumor immune evasion models, our results demonstrate that tumors cells that are deficient in MHC class I antigen presentation can be eliminated by pharmacologic inhibition of RNF31.

Tumor sensitization to CD8$^+$ T and NK cells by RNF31 depletion is relayed through TNF signaling

Secreted cytokines, including TNF and IFN-γ, are established effectors of CD8$^+$ T and NK cell antitumor activity.[51] On the other hand, LUBAC plays a critical role in TNF signaling to regulate cell survival and death.[52,53] Together, this would predict that RNF31 depletion exerts its effects in a TNF-dependent fashion. We therefore ablated its receptor, TNFRSF1A/TNFR1, both in parental and RNF31 knockout tumor cells. In control TNFR1 wild-type cells, RNF31 depletion led to enhanced tumor killing

Figure 3. Pharmacologic inhibition of RNF31 enhances tumor sensitivity to both CD8$^+$ T cell- and NK cell-mediated killing

(A, C, and E) Different cell lines (BLM) (A), (MCF7) (C), and (SW480) (E) were challenged with increasing numbers of MART-1 CD8$^+$ T cells or NK cells, and co-treated with HOIPIN-8 as indicated. Cells were fixed and stained with crystal violet four to five days later.

(B, D, and F) Quantification of (A), (C), and (E); relative killing is normalized to untreated groups. Every T/E ratio shows the average and SD of 3 biological replicates, each with two to three technical replicates. Statistical significance was determined using a two-way ANOVA with Sidak's multiple comparisons test. ***$p < 0.001$.

(G) Percentage of dead cells (total PBMC and subpopulations) after pre-staining with CellTrace Violet dye (CTV), anti-CD3 stimulation, and treatment with HOIPIN-8 (10 μM, 20 μM) or DMSO. n = 4 donors, each donor has three replicates (n = 3 for Tregs as one donor had none). Data are pooled from two independent experiments.

(H) Quantification of cell proliferation of live PBMCs from (G).

(I) Quantification of cell proliferation of CD8$^+$ T, CD4$^+$ T, and Treg cells from (G).

(J and K) The concentration of IFN-γ and TNF in the T cell:tumor cell (BLM) (J) or NK:tumor cell (K) co-culture medium after treatment with HOIPIN-8 (10 μM, 20 μM) or with DMSO. n = 2 donors, each donor has three replicates. Statistical significance was determined using a one-way ANOVA Tukey multiple comparisons test (G–K). *$p < 0.05$, **$p < 0.01$, ***$p < 0.001$.

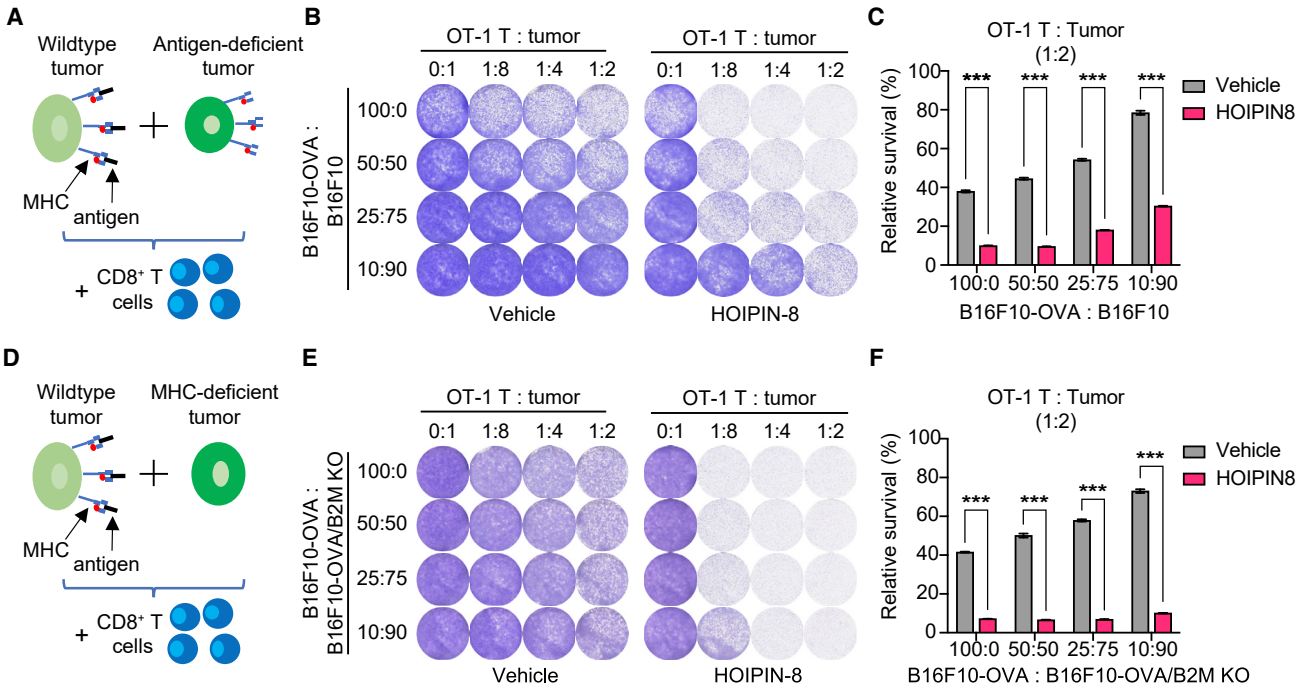

Figure 4. HOIPIN-8 treatment enhances bystander killing of tumor cells deficient in antigen presentation

(A and B) Schematic outline (A) and result (B) of the mixing of wild-type B16F10-OVA cells and antigen-negative B16F10 cells at different ratios (B16F10-OVA:B16F10) followed by OT-1 T cell challenge and HOIPIN-8 treatment.

(C) Quantification of (B) for the 1:2 T cell:tumor cell ratio. n = 3 donors, error bars indicate SD.

(D and E) Schematic outline (D) and result (E) of the mixing of wild-type B16F10-OVA cells and antigen presentation-deficient B2M knockout B16F10-OVA cells at different ratios (B16F10-OVA:B16F10-OVA/B2M KO) followed by OT-1 T cell challenge and HOIPIN-8 treatment.

(F) Quantification of (E) for the 1:2 T cell:tumor cell ratio. n = 3 donors, error bars indicate SD. ***$p < 0.001$ by a one-way ANOVA with Dunnett multiple comparisons test.

by CD8$^+$ T, NK, and TNF treatment (Figures S5A and S5B). In contrast, in TNFR1-depleted cells, RNF31 disruption no longer sensitized tumor cells to immune killing. Incucyte analysis of caspase-3/7 GFP accumulation in live cells confirmed that TNFR1 ablation strongly reduced CD8$^+$ T cell-, NK cell-, and TNF-induced apoptosis in RNF31-deficient tumor cells back to the levels seen in wild-type melanoma cells (Figures 5A and S5C–S5F).

Extending these observations, a TNF neutralizing antibody also blocked tumor sensitivity to CD8$^+$ T and NK cells caused by RNF31 deficiency, similarly to what was observed for TNFR1 depletion (Figures S5G and S5H). Furthermore, biochemical analysis of tumor cells either co-cultured with CD8$^+$ T cells or treated with TNF also demonstrated that, in TNFR1-wild-type cells, RNF31 depletion enhanced caspase-3 cleavage, a hallmark of apoptosis, but this was abolished in TNFR1-deficient cells (Figures S5I and S5J). Thus, our findings demonstrate that TNF is the predominant cytokine accounting for the RNF31-dependent increase in susceptibility to CD8$^+$ T and NK cell elimination.

Genetic and pharmacologic RNF31 inhibition cause loss of A20 and non-canonical IKK complexes from TNF receptor complex I

To further dissect the molecular consequences of both genetic and pharmacologic RNF31 inhibition, we performed proteomic and transcriptional profiling. We showed above that either genetic depletion or pharmacological inhibition of RNF31 sensitizes human BLM melanoma cells to CD8$^+$ T cell, NK cell, and TNF cytotoxicity (Figures 1 and 3). It is established that, immediately downstream of the TNFR, LUBAC mediates linear ubiquitination, enabling canonical nuclear factor κB (NF-κB) gene activation and preventing RIPK1-mediated apoptosis or cell death.[52,54,55] To investigate this in detail, we compared the composition of purified TNFR1 complex in sensitive tumor cells (sgRNF31, HOIPIN-8, and sgRNF31+HOIPIN-8) versus parental resistant tumor cells (sgCtl, vehicle) by tandem mass spectrometry, after confirming all knockouts by western blotting (Figure S5K).

Whereas RBCK1 and SHARPIN, the other two LUBAC components, were in complex with TNFR1 in control and HOIPIN-8-treated conditions, proteomic analysis revealed that they had dissociated in RNF31 genetically depleted cells (Figures 5B and 5C). This analysis also confirmed that HOIPIN-8 treatment does not change the protein level of RNF31, in agreement with data below (Figure 6F) and previous observations by others.[39] Compared with parental cells, the A20 (alias TNFAIP3) complex (A20/TNIP1/TNIP2/TAXIBP1), as well as the non-canonical IKK complex (TBK1/IKBKE/TANK/OPTN), were lacking from the TNFR1 complex in all immune-sensitive tumor cell groups (Figures 5B and 5C). This result is in line with, and extends, the

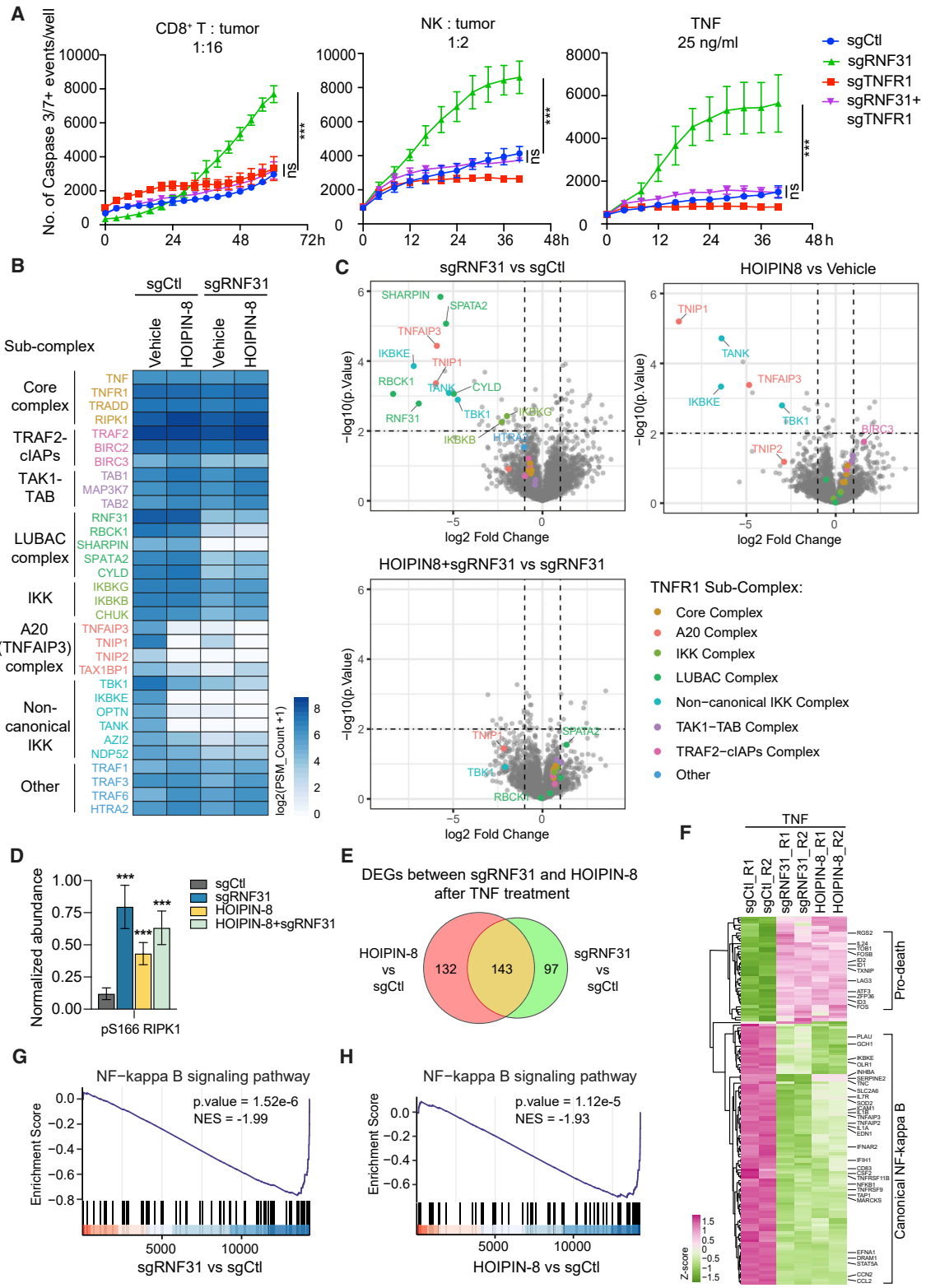

Figure 5. Tumor sensitization to CD8+ T and NK cells by RNF31 depletion is relayed through TNF signaling

(A) Incucyte analysis by caspase-3/7 GFP accumulation for apoptosis of D10 cells expressing indicated sgRNAs and challenged with different numbers of MART-1 CD8+ T cells (left), NK cells (middle), or TNF (right). Quantification of positive caspase-3/7 staining cells per well (n = 3), error bars indicate SD. Other tumor:T cell ratios are shown in Figures S5C–S5F.

(legend continued on next page)

previously proposed roles of LUBAC as key regulators of TNFR1 complex.[56]

The recruitment of both TBK1 and IKKε to the TNFR1 complex is dependent on LUBAC activity.[56] In the absence of LUBAC, RIPK1 kinase is activated to initiate downstream cell death signaling.[57] Indeed, we found increased autophosphorylation of RIPK1 at Ser166, a marker of RIPK1 activity in RNF31-deficient tumor cells (Figures 5D and S5L). Notably, TBK1 and IKBKE were also hits that dropped out in the CRISPR-Cas9 screen when challenged by either $CD8^+$ T cells or NK cells (Figure 1B). Together, these results demonstrate that RNF31 inhibition changes the composition of the TNFR1 complex, specifically the A20 and non-canonical IKK subcomplexes, thereby stimulating TNF-induced death in tumor cells.

Next, we evaluated whether there are transcriptional differences between RNF31-proficient immune-resistant and RNF31-deficient immune-sensitive tumor cells. We stimulated sensitive (sgRNF31- or HOIPIN-8-treated) and resistant (sgCtl, vehicle) BLM tumor cells with TNF for 0 or 6 h and performed RNA sequencing analysis. Principal-component analysis showed clear separation of the sensitive and resistant tumor cells after TNF treatment (Figure S5M). RNF31 inhibition by either sgRNF31 or HOIPIN-8 treatment significantly affected the TNF-induced transcriptional profile (Figure S5N). We identified 143 common significantly differentially expressed genes for RNF31 inhibition by genetic and pharmacologic means (Figure 5E). This gene set distinguished sensitive tumor cells from resistant ones (Figure 5F), with downregulated genes being involved in canonical NF-κB signaling and upregulated genes related to pro-death signaling. GSEA analysis confirmed that sensitive tumor cells exhibited decreased NF-κB signaling activation after TNF treatment (Figures 5G, 5H, and S5O). Thus, tumor cells sensitized by RNF31 inhibition show reduced canonical NF-κB and increased pro-death signatures upon TNF challenge.

HOIPIN-8 increases the sensitivity of multiple tumor types and colon carcinoma organoids to TNF-mediated death

To investigate whether the striking cooperation between RNF31 genetic inactivation and TNF in immune sensitization is observed across different settings, we extended this analysis to multiple human and murine tumor types, as well as colon carcinoma organoids. First, genetic ablation of RNF31 in human melanoma BLM cells, colorectal tumor SW480 cells and breast tumor MCF7 cells strongly sensitized to very low levels of TNF. In parental tumor cells, TNF, even at a high concentration, showed little cytotoxic effect (Figures S6A and S6B), similar to our previous observations.[24] This was recapitulated in multiple murine tumor cell lines: B16F10-OVA melanoma, LL/2-OVA lung cancer, and CT26 and MC38 colon carcinoma (Figures S6C and S6D).

These findings prompted us to next examine whether pharmacological RNF31 inhibition has similar effects. We treated human BLM melanoma cells and SW480 colorectal cells with different doses of TNF and HOIPIN-8. Whereas even 20 μM HOIPIN-8 alone did not affect tumor cell viability, addition of very low amounts of TNF were sufficient to trigger massive cell death (Figures 6A and 6B). We also tested this in several murine tumor cell lines. Again, HOIPIN-8 treatment greatly augmented TNF-mediated cytotoxicity in all four murine tumor cells (Figures 6C and 6D). Specifically, MC38 and LL/2-OVA were almost completely killed under very low concentrations of TNF in combination with HOIPIN-8. Furthermore, we used three different human colon carcinoma organoids (ITO-066, ITO-79, and ITO-111) from patients to test HOIPIN-8 effects at a more clinical level. All three HOIPIN-8-treated organoids showed profoundly increased sensitivity to TNF at very low concentrations (Figures 6E and S6E).

Mechanistically, we observed that in HOIPIN-8-treated organoids, TNF induced more rapid and strong cleavage of caspase-3 than vehicle-treated organoids (Figures 6F and S6F), leading to more apoptosis. These results indicate that RNF31 inhibition increases the susceptibility of tumor organoids to TNF.

High TNF/low RNF31 expression is associated with good prognosis

The mechanistic data above demonstrate that RNF31 is a critical determinant of TNF-mediated tumor killing. We previously showed that TNF expression is increased in the tumor microenvironment after ICB therapy, correlating with improved tumor control.[24] We did not find a correlation between RNF31 expression and ICB response or TNF sensitivity of PDX cell lines (not shown). We therefore investigated whether tumors with high TNF and low RNF31 expression would be associated with a better prognosis. First, we found that RNF31, as well as both of its LUBAC partners, RBCK1 and SHARPIN (both of which

(B) BLM sgCtl or sgRNF31 cells were treated with HOIPIN-8 or vehicle, then stimulated with biotin-TNF (100 ng/mL) for 10 min. TNFR1 complex I proteins were purified by biotin co-immunoprecipitation and analyzed by liquid chromatography-tandem mass spectrometry. The mean PSM count of TNFR1 complex components for three replicates were plotted in a heatmap.

(C) Volcano plots showing relative abundance of TNFR1 complex components in sensitive tumor cells (sgRNF31, HOIPIN-8, sgRNF31+HOIPIN-8) versus resistant tumor cells (sgCtl, vehicle). TNFR1 complex proteins are color coded by subcomplex. Horizontal line indicates $p < 0.01$, vertical lines indicate fold change > 2, n = 3 biological replicates per condition.

(D) Phosphorylation of RIPK1 at Ser166 within the TNFR1 complex measured following biotin-TNF immunoprecipitation-MS in (B). The phosphorylation abundance is normalized to total RIPK1 abundance. n = 3 biological replicates per condition. Error bars indicate SD. ***$p < 0.001$ by unpaired two-sided Student's t test.

(E–H) mRNA sequencing analysis of sensitive (sgRNF31, HOIPIN-8) and resistant (sgCtl, vehicle) BLM tumor cells after exposure to TNF. BLM cells were pre-incubated with either vehicle (DMSO) or HOIPIN-8 for 16 h, followed by stimulation with TNF (100 ng/mL) for 0 and 6 h. n = 2 biological replicates per condition. The Venn diagram (E) represents the number of all significantly differentially expressed genes (DEGs) regulated following 6 h of TNF stimulation between sgRNF31 versus sgCtl and HOIPIN-8 versus sgCtl. The significant DEGs are cut off at fold change > 1.5, FDR < 0.05 in Figure S5N. The heatmap (F) illustrates the normalized expression of significant DEGs from (D) across samples common to genetic and pharmacologic RNF31 inhibition. GSEA plots (G and H) show a downregulated NF-κB signaling pathway in both RNF31 knockout and HOIPIN-8 inhibited cells after TNF treatment.

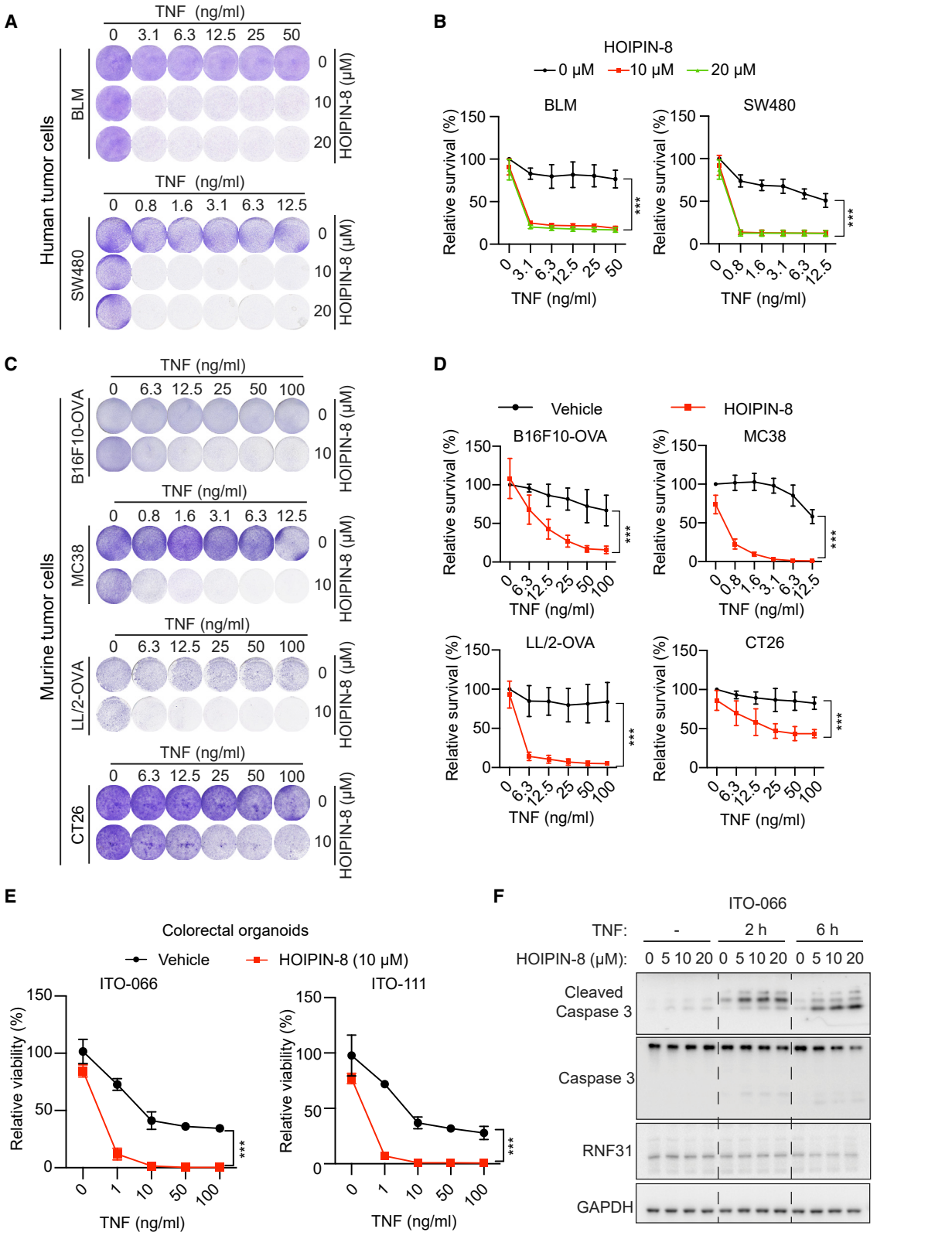

(legend on next page)

sensitized tumor cells to T cells upon their inactivation, similar to RNF31), are commonly expressed to higher levels in tumors than in the adjacent normal tissues (Figures 7A and S7A). This was already seen in stage I tumors and was stable upon tumor progression (Figure S7B). We previously showed that, under baseline conditions, TNF is unlikely to act as a potent antitumor factor, but that upon ablation of specific TNF prosurvival signaling factors, such as TRAF2, tumors are strongly sensitized to TNF.[24] Consistent with this notion, we observed that patients with breast cancer expressing high levels of TNF and low expression of RNF31 had significantly improved survival compared with patients with TNF-high/RNF31-high tumors; this was not seen for the TNF-low tumors (Figure 7B). A similar trend was seen for a melanoma (SKCM) cohort (Figure S7C).

DISCUSSION

Acquired resistance to immunotherapies, including ICB, is a common problem in cancer treatment, creating a dire clinical need for solutions. Common among immunotherapy resistance mechanisms is the loss of antigen presentation. This can be due to deficiencies in MHC class I expression, or other tumor cell components of the antigen presentation machinery, such as B2M, or the antigen itself, enabling tumors to hide under the $CD8^+$ T cell radar. At least part of this mechanism of immune evasion can be counteracted by NK cells, since MHC class I loss alleviates one mechanism of NK cell inhibition.[58] However, NK cell activation is complex and apparently does not account for a sufficiently robust defense mechanism in many (immunotherapy-treated) patients. Therefore, we performed parallel genome-wide CRISPR-Cas9 screens to identify genes whose inactivation sensitizes tumor cells not only to adaptive $CD8^+$ T cells (recognizing antigen-presenting cells) but also to innate NK cells (recognizing antigen presentation-deficient tumor cells).

This approach identified all components of LUBAC, including the E3 ubiquitin ligase RNF31. LUBAC is recruited to cell membrane-bound TNF receptor complex I, upon polyubiquitination of several associated proteins by BIRC2/3.[59–61] There, it conjugates linear polyubiquitin to IKBKG and other components, thereby contributing to the stability of the complex.[59,62] Extending these notions, we demonstrate that either genetic depletion or inhibition of RNF31 with a small-molecule compound greatly sensitizes tumor cells of different indications to both adaptive and innate immune cells. Our proteomic analysis shows that RNF31 inhibition causes a highly specific disruption of the cell ligand-bound TNF receptor complex I, leading to the loss of A20 and non-canonical IKK complexes. Together with our gene expression analysis, these results indicate that apoptosis is enhanced through reduced canonical NF-κB signaling.

These findings are in keeping with our recent report that selective inactivation of components of the prosurvival arm downstream of TNFR signaling, for example, by loss of TRAF2, is an effective means to sensitize tumor cells to TNF.[24] Moreover, we showed that tumors from patients who fail to respond to ICB have much lower levels of TNF in the tumor microenvironment. We thus proposed that it may be clinically beneficial to sensitize tumors to such low levels of TNF. Although our data clearly show a major role for TNF in this context, we cannot exclude that IFN-γ may cooperate. This, and our other findings are in full agreement with, and extend our previous findings and those of others,[34,37,63,64] demonstrating that RNF31 inhibition strongly sensitizes to very low amounts of TNF.

In our $CD8^+$ T cell and NK cell screens, we observed that as many as 192 genes were jointly depleted and 51 enriched. The TNF and autophagy pathways stood out in both arms, which was expected, because of their established roles in immune cell-mediated cytotoxicity.[14,24,31,34,36,65,66] We also found genes specific for either NK cell killing (235 genes) or $CD8^+$ T cell killing (483 genes). IFNGR2, JAK2, STAT1, IRF1, and B2M were enriched in the $CD8^+$ T cell arm, but not in the NK cell arm. This is in agreement with the notion that the IFN-γ and antigen presentation pathways are specifically important for $CD8^+$ T cell killing. LTBR, a member of the TNF receptor superfamily,[67] was also specifically enriched in the NK cell arm, again illustrating that it is possible to inhibit common mediators of adaptive and innate immune killing.

Our results also highlight the power of bystander killing. This activity is highly relevant for the immune elimination of tumors, or tumor fractions, that have lost or downregulated components of their antigen presentation machinery, thereby allowing them to escape from $CD8^+$ T cell attack, whether during the process of tumorigenesis or on immunotherapy.[5,50] Bystander killing is gaining increasing interest, and it has been recently shown to occur over large distances *in vivo*.[49] Here, we show that HOIPIN-8 treatment greatly enhances bystander killing of antigen loss and antigen presentation machinery-deficient tumor cells: as few as 10% antigen-positive cells were sufficient to cause immune elimination of 90% antigen-negative cells when co-treated with TNF and HOIPIN-8 (but not either alone). These results raise the possibility that this strategy may be exploited therapeutically, specifically for heterogeneous tumors comprising antigen presentation-proficient and -deficient fractions, which is a common phenomenon.[9,45–47,50,68–70]

Figure 6. HOIPIN-8 increases the sensitivity of multiple tumor types and colon carcinoma organoids to TNF-mediated death

(A and B) Human BLM and SW480 tumor cells in the presence of HOIPIN-8 or vehicle challenged with increasing amounts of TNF as indicated (A). The relative survival is normalized to the untreated group (B). Every dose of TNF shows the average and SD of 2–3 biological replicates, each with three technical replicates. Cells were fixed and stained with crystal violet 4–5 days later.

(C and D) Murine B16F10-OVA, MC38, LL/2-OVA, and CT26 tumor cells in the presence of HOIPIN-8 or vehicle challenged with increasing amount of TNF as indicated (C). Quantification of (C), the relative survival is normalized to untreated group (D). Every dose of TNF shows the average and SD of 3 biological replicates, each with three technical replicates.

(E) Viability of two colorectal organoids from independent patients (ITO-066 and ITO-111) in the presence of HOIPIN-8 or vehicle after treatment with increasing concentrations of TNF. Relative viability measured by CellTiter-Glo 3D is normalized to the vehicle control group. Every dose of TNF shows the average and SD of 2 technical replicates for each of the organoids from three patients; see also Figure S6E.

(F) Western blot analysis of colorectal organoids from tumor ITO-066 in the presence of HOIPIN-8 or vehicle after exposure to TNF (100 ng/mL) for 0, 2, and 6 h. Statistical significance was determined using a two-way ANOVA with Sidak's multiple comparisons test for (B, D, and E). ***$p < 0.001$.

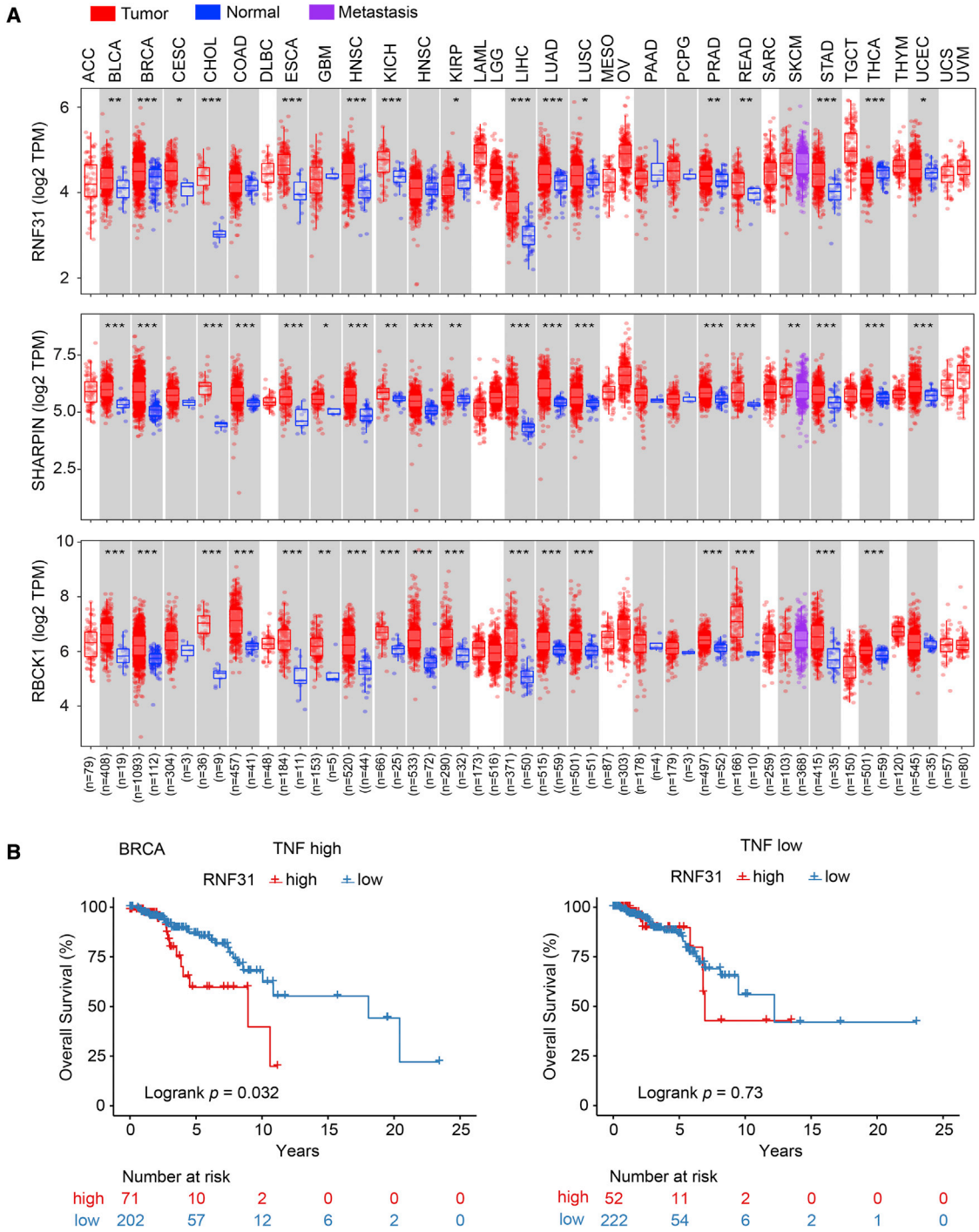

Figure 7. High TNF/low RNF31 expression is associated with good prognosis

(A) Expression of RNF31, SHARPIN, and RBCK1 in primary tumors (red), metastases (purple), and related normal tissue (blue) among TCGA cancer types. Data are represented as log2(TPM) and were queried from TIMER2.0. The statistical significance was computed by the Wilcoxon test. *$p < 0.05$, **$p < 0.01$, ***$p < 0.001$. (B) Kaplan-Meier overall survival analysis for breast cancer cohort from TCGA (BRCA) divided in top and bottom quartile TNF-expressing tumors distributed over the top quartile and the remainder (75%) of RNF31-expressing tumors. p value was computed by log rank test.

Several small-molecule approaches have been used to target RNF31, whether directly or indirectly.[63,71–73] HOIPIN-1 was recently identified as a LUBAC chemical inhibitor through high-throughput screening.[40] HOIPIN-8 is a derivative, showing enhanced inhibitory activities toward LUBAC without cytotoxicity,[38] which we confirmed here. HOIPIN-8 specifically targets

RNF31 through attaching to the catalytic Cys885 residue.[39] Therefore, we used HOIPIN-8 to inhibit RNF31, which enabled us to demonstrate that pharmacologic inhibition of RNF31 strongly sensitizes tumor cells, of different tissue origins, to both $CD8^+$ T cell- and NK cell-mediated killing. Although HOIPIN-8 showed some effects on the immune cell compartment, it did not result in reduced $CD8^+$ T cell activity in the conditions we investigated.

In an attempt to translate these findings to a preclinical *in vivo* setting, we found that the blood concentration of HOIPIN-8 upon intravenous administration is very low, precluding pharmacologic preclinical validation. Therefore, we used genetic ablation instead, demonstrating that RNF31 loss provokes tumor immune clearance in two murine cancer graft immune-proficient models, B16F10-OVA melanoma and MC38 colon cancer. Furthermore, we validated the striking cooperative activities of HOIPIN-8 and TNF in multiple patient-derived colorectal organoids. In this context it is noteworthy that RNF31 also contributes, to different degrees, to tumor expansion *in vivo*, on top of its role in desensitizing tumors to immune attack, whereas no difference was seen *in vitro*. A possible explanation for the latter observation is that the trace amounts of TNF that are present in the serum of NSG mice[74] are sufficient for RNF31-deficient tumor cells to die, which would be consistent with our previous results.[24] From a clinical point of view, simultaneous inhibition of these two roles of RNF31 may be a beneficial trait.

Our results merit a preclinical investigation into the applicability of enhancing TNF-mediated killing in general and RNF31 inhibition in particular in immuno-oncology. In this respect, it is noteworthy that a second mitochondrial-derived activator of caspases (SMAC) mimetic, birinapant, targeting inhibitor of apoptosis protein family proteins, has been explored in combination with anti-PD-1 in a clinical trial (NCT02587962), but this was terminated based on a futility analysis. Indeed, we propose that RNF31 may serve as a new and attractive pharmacological target that may be used especially in TNF-low tumors as well as tumors that are heterogeneous for their ability to present tumor antigens, to empower both $CD8^+$ T cell and NK cell antitumor activity.

Limitations of the study

Although our study has a clear translational outlook, it is important to note that the currently available RNF31 inhibitor HOIPIN-8 has a poor *in vivo* profile in mice, precluding an assessment of *in vivo* antitumor activity. Furthermore, we observed an effect of HOIPIN-8 on the immune cell compartment. Although this mostly related to non-T cells and did not impact on $CD8^+$ T cell cytokine secretion and antitumor activity, it will be important to investigate the possibility of toxicity of any RNF31 inhibition *in vivo*.

STAR★METHODS

Detailed methods are provided in the online version of this paper and include the following:

SUPPLEMENTAL INFORMATION

Supplemental information can be found online at https://doi.org/10.1016/j.xcrm.2022.100655.

ACKNOWLEDGMENTS

We thank all members of the Peeper laboratory for helpful discussions. We thank the Animal facility, Cytometry facility, and Genomics core facility of NKI for support. We thank Joleen Traets and Alex van Vliet for help with bioinformatic analyses, and Disha Rao for help with FACS analysis. This work was supported by LSH-TKI grant LSHM20019, Oncode TDF grant P2019-0060, and Oncode base funding to D.S.P.

AUTHOR CONTRIBUTIONS

X.K., M.A.L., and D.S.P. conceived the project. X.K. and M.A.L. performed the screen. Z.Z. and T.K. performed bioinformatic analyses. M.A.L., B.d.B., and S.E.v.H.-v.V. performed *in vivo* experiments. P.W.v.d.H., E.E.V., and Z.Z. were responsible for organoids experiments. Z.Z. and X.K. performed all other experiments. K.E.S. and M.A. performed mass spectrometric analysis. S.K. performed the IHC quantification. N.L.V., S.E.v.H.-v.V., E.P.H., D.W.V., G.A., and B.B. provided technical support. G.A. assisted with statistical analyses. Z.Z., X.K., and D.S.P. wrote the manuscript. All authors revised and approved the manuscript. The project was supervised by D.S.P.

DECLARATION OF INTERESTS

D.S.P. is co-founder, shareholder, and advisor of Immagene. M.A.L. is co-founder, shareholder, and CEO of Immagene. The other authors declare no competing interests.

Received: October 22, 2021
Revised: February 17, 2022
Accepted: May 17, 2022
Published: June 9, 2022

REFERENCES

1. Larkin, J., Chiarion-Sileni, V., Gonzalez, R., Grob, J.J., Rutkowski, P., Lao, C.D., Cowey, C.L., Schadendorf, D., Wagstaff, J., Dummer, R., et al. (2019). Five-year survival with combined nivolumab and ipilimumab in advanced melanoma. N. Engl. J. Med. *381*, 1535–1546. https://doi.org/10.1056/NEJMoa1910836.
2. Weber, J., Mandala, M., Del Vecchio, M., Gogas, H.J., Arance, A.M., Cowey, C.L., Dalle, S., Schenker, M., Chiarion-Sileni, V., Marquez-Rodas, I., et al. (2017). Adjuvant nivolumab versus ipilimumab in resected stage III or IV melanoma. N. Engl. J. Med. *377*, 1824–1835. https://doi.org/10.1056/NEJMoa1709030.
3. Sharma, P., Hu-Lieskovan, S., Wargo, J.A., and Ribas, A. (2017). Primary, adaptive, and acquired resistance to cancer immunotherapy. Cell *168*, 707–723. https://doi.org/10.1016/j.cell.2017.01.017.
4. Gubin, M.M., Zhang, X., Schuster, H., Caron, E., Ward, J.P., Noguchi, T., Ivanova, Y., Hundal, J., Arthur, C.D., Krebber, W.J., et al. (2014). Checkpoint blockade cancer immunotherapy targets tumour-specific mutant antigens. Nature *515*, 577–581. https://doi.org/10.1038/nature13988.
5. Sade-Feldman, M., Jiao, Y.J., Chen, J.H., Rooney, M.S., Barzily-Rokni, M., Eliane, J.P., Bjorgaard, S.L., Hammond, M.R., Vitzthum, H., Blackmon, S.M., et al. (2017). Resistance to checkpoint blockade therapy through inactivation of antigen presentation. Nat. Commun. *8*, 1136. https://doi.org/10.1038/s41467-017-01062-w.
6. Marincola, F.M., Jaffee, E.M., Hicklin, D.J., and Ferrone, S. (2000). Escape of human solid tumors from T-cell recognition: molecular mechanisms and functional significance. Adv. Immunol. *74*, 181–273. https://doi.org/10.1016/s0065-2776(08)60911-6.
7. Sucker, A., Zhao, F., Real, B., Heeke, C., Bielefeld, N., Maβen, S., Horn, S., Moll, I., Maltaner, R., Horn, P.A., et al. (2014). Genetic evolution of T-cell resistance in the course of melanoma progression. Clin. Cancer Res. *20*, 6593–6604. https://doi.org/10.1158/1078-0432.CCR-14-0567.
8. Burr, M.L., Sparbier, C.E., Chan, K.L., Chan, Y.C., Kersbergen, A., Lam, E.Y.N., Azidis-Yates, E., Vassiliadis, D., Bell, C.C., Gilan, O., et al. (2019). An evolutionarily conserved function of polycomb silences the MHC class I antigen presentation pathway and enables immune evasion in cancer. Cancer Cell *36*, 385–401.e8. https://doi.org/10.1016/j.ccell.2019.08.008.
9. del Campo, A.B., Kyte, J.A., Carretero, J., Zinchencko, S., Mendez, R., Gonzalez-Aseguinolaza, G., Ruiz-Cabello, F., Aamdal, S., Gaudernack, G., Garrido, F., and Aptsiauri, N. (2014). Immune escape of cancer cells with beta2-microglobulin loss over the course of metastatic melanoma. Int. J. Cancer *134*, 102–113. https://doi.org/10.1002/ijc.28338.
10. McGranahan, N., Rosenthal, R., Hiley, C.T., Rowan, A.J., Watkins, T.B.K., Wilson, G.A., Birkbak, N.J., Veeriah, S., Van Loo, P., Herrero, J., et al. (2017). Allele-specific HLA loss and immune escape in lung cancer evolution. Cell *171*, 1259–1271.e11. https://doi.org/10.1016/j.cell.2017.10.001.
11. Rosenthal, R., Cadieux, E.L., Salgado, R., Bakir, M.A., Moore, D.A., Hiley, C.T., Lund, T., Tanic, M., Reading, J.L., Joshi, K., et al. (2019). Neoantigen-directed immune escape in lung cancer evolution. Nature *567*, 479–485. https://doi.org/10.1038/s41586-019-1032-7.
12. Mujal, A.M., Delconte, R.B., and Sun, J.C. (2021). Natural killer cells: from innate to adaptive features. Annu. Rev. Immunol. *39*, 417–447. https://doi.org/10.1146/annurev-immunol-101819-074948.
13. Prager, I., Liesche, C., van Ooijen, H., Urlaub, D., Verron, Q., Sandstrom, N., Fasbender, F., Claus, M., Eils, R., Beaudouin, J., et al. (2019). NK cells switch from granzyme B to death receptor-mediated cytotoxicity during serial killing. J. Exp. Med. *216*, 2113–2127. https://doi.org/10.1084/jem.20181454.
14. Sordo-Bahamonde, C., Lorenzo-Herrero, S., Payer, A.R., Gonzalez, S., and Lopez-Soto, A. (2020). Mechanisms of apoptosis resistance to NK cell-mediated cytotoxicity in cancer. Int. J. Mol. Sci. *21*, 3726. https://doi.org/10.3390/ijms21103726.
15. Chiossone, L., Dumas, P.Y., Vienne, M., and Vivier, E. (2018). Natural killer cells and other innate lymphoid cells in cancer. Nat. Rev. Immunol. *18*, 671–688. https://doi.org/10.1038/s41577-018-0061-z.
16. Myers, J.A., and Miller, J.S. (2021). Exploring the NK cell platform for cancer immunotherapy. Nat. Rev. Clin. Oncol. *18*, 85–100. https://doi.org/10.1038/s41571-020-0426-7.
17. Bryceson, Y.T., March, M.E., Ljunggren, H.G., and Long, E.O. (2006). Activation, coactivation, and costimulation of resting human natural killer cells. Immunol. Rev. *214*, 73–91. https://doi.org/10.1111/j.1600-065X.2006.00457.x.
18. Platonova, S., Cherfils-Vicini, J., Damotte, D., Crozet, L., Vieillard, V., Validire, P., Andre, P., Dieu-Nosjean, M.C., Alifano, M., Regnard, J.F., et al. (2011). Profound coordinated alterations of intratumoral NK cell phenotype and function in lung carcinoma. Cancer Res. *71*, 5412–5422. https://doi.org/10.1158/0008-5472.CAN-10-4179.
19. Bald, T., Krummel, M.F., Smyth, M.J., and Barry, K.C. (2020). The NK cell-cancer cycle: advances and new challenges in NK cell-based immunotherapies. Nat. Immunol. *21*, 835–847. https://doi.org/10.1038/s41590-020-0728-z.
20. Melsen, J.E., Lugthart, G., Lankester, A.C., and Schilham, M.W. (2016). Human circulating and tissue-resident CD56(bright) natural killer cell populations. Front. Immunol. *7*, 262. https://doi.org/10.3389/fimmu.2016.00262.
21. Shimasaki, N., Jain, A., and Campana, D. (2020). NK cells for cancer immunotherapy. Nat. Rev. Drug Discov. *19*, 200–218. https://doi.org/10.1038/s41573-019-0052-1.
22. Doubrovina, E.S., Doubrovin, M.M., Vider, E., Sisson, R.B., O'Reilly, R.J., Dupont, B., and Vyas, Y.M. (2003). Evasion from NK cell immunity by MHC class I chain-related molecules expressing colon adenocarcinoma. J. Immunol. *171*, 6891–6899. https://doi.org/10.4049/jimmunol.171.12.6891.
23. Raulet, D.H., Gasser, S., Gowen, B.G., Deng, W., and Jung, H. (2013). Regulation of ligands for the NKG2D activating receptor. Annu. Rev. Immunol. *31*, 413–441. https://doi.org/10.1146/annurev-immunol-032712-095951.
24. Vredevoogd, D.W., Kuilman, T., Ligtenberg, M.A., Boshuizen, J., Stecker, K.E., de Bruijn, B., Krijgsman, O., Huang, X., Kenski, J.C.N., Lacroix, R., et al. (2019). Augmenting immunotherapy impact by lowering tumor TNF cytotoxicity threshold. Cell *178*, 585–599.e15. https://doi.org/10.1016/j.cell.2019.06.014.
25. Gomez-Eerland, R., Nuijen, B., Heemskerk, B., van Rooij, N., van den Berg, J.H., Beijnen, J.H., Uckert, W., Kvistborg, P., Schumacher, T.N., Haanen, J.B., and Jorritsma, A. (2014). Manufacture of gene-modified human T-cells with a memory stem/central memory phenotype. Hum. Gene Ther. Methods *25*, 277–287. https://doi.org/10.1089/hgtb.2014.004.
26. Jorritsma, A., Gomez-Eerland, R., Dokter, M., van de Kasteele, W., Zoet, Y.M., Doxiadis, I.I.N., Rufer, N., Romero, P., Morgan, R.A., Schumacher, T.N.M., and Haanen, J.B.A.G. (2007). Selecting highly affine and well-expressed TCRs for gene therapy of melanoma. Blood *110*, 3564–3572. https://doi.org/10.1182/blood-2007-02-075010.
27. Yagita, M., Huang, C.L., Umehara, H., Matsuo, Y., Tabata, R., Miyake, M., Konaka, Y., and Takatsuki, K. (2000). A novel natural killer cell line (KHYG-1) from a patient with aggressive natural killer cell leukemia carrying a p53 point mutation. Leukemia *14*, 922–930. https://doi.org/10.1038/sj.leu.2401769.
28. Suck, G., Branch, D.R., Smyth, M.J., Miller, R.G., Vergidis, J., Fahim, S., and Keating, A. (2005). KHYG-1, a model for the study of enhanced natural killer cell cytotoxicity. Exp. Hematol. *33*, 1160–1171. https://doi.org/10.1016/j.exphem.2005.06.024.

29. Dahlberg, C.I.M., Sarhan, D., Chrobok, M., Duru, A.D., and Alici, E. (2015). Natural killer cell-based therapies targeting cancer: possible strategies to gain and sustain anti-tumor activity. Front. Immunol. *6*, 605. https://doi.org/10.3389/fimmu.2015.00605.

30. Shalem, O., Sanjana, N.E., Hartenian, E., Shi, X., Scott, D.A., Mikkelsen, T.S., Heckl, D., Ebert, B.L., Root, D.E., Doench, J.G., and Zhang, F. (2014). Genome-scale CRISPR-Cas9 knockout screening in human cells. Science *343*, 84–87. https://doi.org/10.1126/science.1247005.

31. Kearney, C.J., Vervoort, S.J., Hogg, S.J., Ramsbottom, K.M., Freeman, A.J., Lalaoui, N., Pijpers, L., Michie, J., Brown, K.K., Knight, D.A., et al. (2018). Tumor immune evasion arises through loss of TNF sensitivity. Sci. Immunol. *3*, eaar3451. https://doi.org/10.1126/sciimmunol.aar3451.

32. Patel, S.J., Sanjana, N.E., Kishton, R.J., Eidizadeh, A., Vodnala, S.K., Cam, M., Gartner, J.J., Jia, L., Steinberg, S.M., Yamamoto, T.N., et al. (2017). Identification of essential genes for cancer immunotherapy. Nature *548*, 537–542. https://doi.org/10.1038/nature23477.

33. Dubrot, J., Lane-Reticker, S.K., Kessler, E.A., Ayer, A., Mishra, G., Wolfe, C.H., Zimmer, M.D., Du, P.P., Mahapatra, A., Ockerman, K.M., et al. (2021). In vivo screens using a selective CRISPR antigen removal lentiviral vector system reveal immune dependencies in renal cell carcinoma. Immunity *54*, 571–585.e6. https://doi.org/10.1016/j.immuni.2021.01.001.

34. Young, T.M., Reyes, C., Pasnikowski, E., Castanaro, C., Wong, C., Decker, C.E., Chiu, J., Song, H., Wei, Y., Bai, Y., et al. (2020). Autophagy protects tumors from T cell–mediated cytotoxicity via inhibition of TNFα-induced apoptosis. Sci. Immunol. *5*, eabb9561. https://doi.org/10.1126/sciimmunol.abb9561.

35. Lawson, K.A., Sousa, C.M., Zhang, X., Kim, E., Akthar, R., Caumanns, J.J., Yao, Y., Mikolajewicz, N., Ross, C., Brown, K.R., et al. (2020). Functional genomic landscape of cancer-intrinsic evasion of killing by T cells. Nature *586*, 120–126. https://doi.org/10.1038/s41586-020-2746-2.

36. Zhu, X.G., Chudnovskiy, A., Baudrier, L., Prizer, B., Liu, Y., Ostendorf, B.N., Yamaguchi, N., Arab, A., Tavora, B., Timson, R., et al. (2021). Functional genomics in vivo reveal metabolic dependencies of pancreatic cancer cells. Cell Metab. *33*, 211–221.e6. https://doi.org/10.1016/j.cmet.2020.10.017.

37. Freeman, A.J., Vervoort, S.J., Ramsbottom, K.M., Kelly, M.J., Michie, J., Pijpers, L., Johnstone, R.W., Kearney, C.J., and Oliaro, J. (2019). Natural killer cells suppress T cell-associated tumor immune evasion. Cell Rep. *28*, 2784–2794.e5. https://doi.org/10.1016/j.celrep.2019.08.017.

38. Katsuya, K., Oikawa, D., Iio, K., Obika, S., Hori, Y., Urashima, T., Ayukawa, K., and Tokunaga, F. (2019). Small-molecule inhibitors of linear ubiquitin chain assembly complex (LUBAC), HOIPINs, suppress NF-κB signaling. Biochem. Biophys. Res. Commun. *509*, 700–706. https://doi.org/10.1016/j.bbrc.2018.12.164.

39. Oikawa, D., Sato, Y., Ohtake, F., Komakura, K., Hanada, K., Sugawara, K., Terawaki, S., Mizukami, Y., Phuong, H.T., Iio, K., et al. (2020). Molecular bases for HOIPINs-mediated inhibition of LUBAC and innate immune responses. Commun. Biol. *3*, 163. https://doi.org/10.1038/s42003-020-0882-8.

40. Katsuya, K., Hori, Y., Oikawa, D., Yamamoto, T., Umetani, K., Urashima, T., Kinoshita, T., Ayukawa, K., Tokunaga, F., and Tamaru, M. (2018). High-throughput screening for linear ubiquitin chain assembly complex (LUBAC) selective inhibitors using homogenous time-resolved fluorescence (HTRF)-Based assay system. SLAS Discov. *23*, 1018–1029. https://doi.org/10.1177/2472555218793066.

41. Sasaki, K., and Iwai, K. (2015). Roles of linear ubiquitinylation, a crucial regulator of NF-κB and cell death, in the immune system. Immunol. Rev. *266*, 175–189. https://doi.org/10.1111/imr.12308.

42. Zhu, F., Yi, G., Liu, X., Zhu, F., Zhao, A., Wang, A., Zhu, R., Chen, Z., Zhao, B., Fang, S., et al. (2018). Ring finger protein 31-mediated atypical ubiquitination stabilizes forkhead box P3 and thereby stimulates regulatory T-cell function. J. Biol. Chem. *293*, 20099–20111. https://doi.org/10.1074/jbc.RA118.005802.

43. Teh, C.E., Lalaoui, N., Jain, R., Policheni, A.N., Heinlein, M., Alvarez-Diaz, S., Sheridan, J.M., Rieser, E., Deuser, S., Darding, M., et al. (2016). Linear ubiquitin chain assembly complex coordinates late thymic T-cell differentiation and regulatory T-cell homeostasis. Nat. Commun. *7*, 13353. https://doi.org/10.1038/ncomms13353.

44. Restifo, N.P., Marincola, F.M., Kawakami, Y., Taubenberger, J., Yannelli, J.R., and Rosenberg, S.A. (1996). Loss of functional beta2-microglobulin in metastatic melanomas from five patients receiving immunotherapy. J. Natl. Cancer Inst. *88*, 100–108. https://doi.org/10.1093/jnci/88.2.100.

45. Janikovits, J., Muller, M., Krzykalla, J., Korner, S., Echterdiek, F., Lahrmann, B., Grabe, N., Schneider, M., Benner, A., Doeberitz, M.V.K., and Kloor, M. (2018). High numbers of PDCD1 (PD-1)-positive T cells and B2M mutations in microsatellite-unstable colorectal cancer. Oncoimmunology *7*, e1390640. https://doi.org/10.1080/2162402X.2017.1390640.

46. Le, D.T., Durham, J.N., Smith, K.N., Wang, H., Bartlett, B.R., Aulakh, L.K., Lu, S., Kemberling, H., Wilt, C., Luber, B.S., et al. (2017). Mismatch repair deficiency predicts response of solid tumors to PD-1 blockade. Science *357*, 409–413. https://doi.org/10.1126/science.aan6733.

47. Zaretsky, J.M., Garcia-Diaz, A., Shin, D.S., Escuin-Ordinas, H., Hugo, W., Hu-Lieskovan, S., Torrejon, D.Y., Abril-Rodriguez, G., Sandoval, S., Barthly, L., et al. (2016). Mutations associated with acquired resistance to PD-1 blockade in melanoma. N. Engl. J. Med. *375*, 819–829. https://doi.org/10.1056/NEJMoa1604958.

48. Dhatchinamoorthy, K., Colbert, J.D., and Rock, K.L. (2021). Cancer immune evasion through loss of MHC class I antigen presentation. Front. Immunol. *12*, 636568. https://doi.org/10.3389/fimmu.2021.636568.

49. Hoekstra, M.E., Bornes, L., Dijkgraaf, F.E., Philips, D., Pardieck, I.N., Toebes, M., Thommen, D.S., van Rheenen, J., and Schumacher, T.N.M. (2020). Long-distance modulation of bystander tumor cells by CD8+ T-cell-secreted IFN-γ. Nat. Cancer *1*, 291–301. https://doi.org/10.1038/s43018-020-0036-4.

50. Spiotto, M.T., Rowley, D.A., and Schreiber, H. (2004). Bystander elimination of antigen loss variants in established tumors. Nat. Med. *10*, 294–298. https://doi.org/10.1038/nm999.

51. Waldmann, T.A. (2018). Cytokines in cancer immunotherapy. Cold Spring Harb. Perspect. Biol. *10*, a028472. https://doi.org/10.1101/cshperspect.a028472.

52. Spit, M., Rieser, E., and Walczak, H. (2019). Linear ubiquitination at a glance. J. Cell Sci. *132*, jcs208512. https://doi.org/10.1242/jcs.208512.

53. Hrdinka, M., and Gyrd-Hansen, M. (2017). The met1-linked ubiquitin machinery: emerging themes of (De)regulation. Mol. Cell *68*, 265–280. https://doi.org/10.1016/j.molcel.2017.09.001.

54. Annibaldi, A., and Meier, P. (2018). Checkpoints in TNF-induced cell death: implications in inflammation and cancer. Trends Mol. Med. *24*, 49–65. https://doi.org/10.1016/j.molmed.2017.11.002.

55. Gerlach, B., Cordier, S.M., Schmukle, A.C., Emmerich, C.H., Rieser, E., Haas, T.L., Webb, A.I., Rickard, J.A., Anderton, H., Wong, W.W.L., et al. (2011). Linear ubiquitination prevents inflammation and regulates immune signalling. Nature *471*, 591–596. https://doi.org/10.1038/nature09816.

56. Lafont, E., Draber, P., Rieser, E., Reichert, M., Kupka, S., de Miguel, D., Draberova, H., von Massenhausen, A., Bhamra, A., Henderson, S., et al. (2018). TBK1 and IKKε prevent TNF-induced cell death by RIPK1 phosphorylation. Nat. Cell Biol. *20*, 1389–1399. https://doi.org/10.1038/s41556-018-0229-6.

57. Laurien, L., Nagata, M., Schunke, H., Delanghe, T., Wiederstein, J.L., Kumari, S., Schwarzer, R., Corona, T., Kruger, M., Bertrand, M.J.M., et al. (2020). Autophosphorylation at serine 166 regulates RIP kinase

1-mediated cell death and inflammation. Nat. Commun. *11*, 1747. https://doi.org/10.1038/s41467-020-15466-8.

58. Souza-Fonseca-Guimaraes, F., Cursons, J., and Huntington, N.D. (2019). The emergence of natural killer cells as a major target in cancer immunotherapy. Trends Immunol. *40*, 142–158. https://doi.org/10.1016/j.it.2018.12.003.

59. Haas, T.L., Emmerich, C.H., Gerlach, B., Schmukle, A.C., Cordier, S.M., Rieser, E., Feltham, R., Vince, J., Warnken, U., Wenger, T., et al. (2009). Recruitment of the linear ubiquitin chain assembly complex stabilizes the TNF-R1 signaling complex and is required for TNF-mediated gene induction. Mol. Cell *36*, 831–844. https://doi.org/10.1016/j.molcel.2009.10.013.

60. Bertrand, M.J., Milutinovic, S., Dickson, K.M., Ho, W.C., Boudreault, A., Durkin, J., Gillard, J.W., Jaquith, J.B., Morris, S.J., and Barker, P.A. (2008). cIAP1 and cIAP2 facilitate cancer cell survival by functioning as E3 ligases that promote RIP1 ubiquitination. Mol. Cell *30*, 689–700. https://doi.org/10.1016/j.molcel.2008.05.014.

61. Varfolomeev, E., Goncharov, T., Fedorova, A.V., Dynek, J.N., Zobel, K., Deshayes, K., Fairbrother, W.J., and Vucic, D. (2008). c-IAP1 and c-IAP2 are critical mediators of tumor Necrosis factor α (TNFα)-induced NF-κB activation. J. Biol. Chem. *283*, 24295–24299. https://doi.org/10.1074/jbc.C800128200.

62. Schlicher, L., Wissler, M., Preiss, F., Brauns-Schubert, P., Jakob, C., Dumit, V., Borner, C., Dengjel, J., and Maurer, U. (2016). SPATA 2 promotes CYLD activity and regulates TNF -induced NF -κB signaling and cell death. EMBO Rep. *17*, 1485–1497. https://doi.org/10.15252/embr.201642592.

63. Jo, T., Nishikori, M., Kogure, Y., Arima, H., Sasaki, K., Sasaki, Y., Nakagawa, T., Iwai, F., Momose, S., Shiraishi, A., et al. (2020). LUBAC accelerates B-cell lymphomagenesis by conferring resistance to genotoxic stress on B cells. Blood *136*, 684–697. https://doi.org/10.1182/blood.2019002654.

64. Freeman, A.J., Vervoort, S.J., Michie, J., Ramsbottom, K.M., Silke, J., Kearney, C.J., and Oliaro, J. (2021). HOIP limits anti-tumor immunity by protecting against combined TNF and IFN-gamma-induced apoptosis. EMBO Rep. *22*, e53391. https://doi.org/10.15252/embr.202153391.

65. Zhong, Z., Sanchez-Lopez, E., and Karin, M. (2016). Autophagy, inflammation, and immunity: a troika governing cancer and its treatment. Cell *166*, 288–298. https://doi.org/10.1016/j.cell.2016.05.051.

66. Levine, B., Mizushima, N., and Virgin, H.W. (2011). Autophagy in immunity and inflammation. Nature *469*, 323–335. https://doi.org/10.1038/nature09782.

67. Rooney, I.A., Butrovich, K.D., Glass, A.A., Borboroglu, S., Benedict, C.A., Whitbeck, J.C., Cohen, G.H., Eisenberg, R.J., and Ware, C.F. (2000). The lymphotoxin-beta receptor is necessary and sufficient for LIGHT-mediated apoptosis of tumor cells. J. Biol. Chem. *275*, 14307–14315. https://doi.org/10.1074/jbc.275.19.14307.

68. Ryschich, E., Notzel, T., Hinz, U., Autschbach, F., Ferguson, J., Simon, I., Weitz, J., Frohlich, B., Klar, E., Buchler, M.W., and Schmidt, J. (2005). Control of T-cell-mediated immune response by HLA class I in human pancreatic carcinoma. Clin. Cancer Res. *11*, 498–504.

69. Garrido, F., Ruiz-Cabello, F., and Aptsiauri, N. (2017). Rejection versus escape: the tumor MHC dilemma. Cancer Immunol. Immunother. *66*, 259–271. https://doi.org/10.1007/s00262-016-1947-x.

70. Cabrera, T., Lopez-Nevot, M.A., Gaforio, J.J., Ruiz-Cabello, F., and Garrido, F. (2003). Analysis of HLA expression in human tumor tissues. Cancer Immunol. Immunother. *52*, 1–9. https://doi.org/10.1007/s00262-002-0332-0.

71. Johansson, H., Isabella Tsai, Y.C., Fantom, K., Chung, C.W., Kumper, S., Martino, L., Thomas, D.A., Eberl, H.C., Muelbaier, M., House, D., and Rittinger, K. (2019). Fragment-based covalent ligand screening enables rapid discovery of inhibitors for the RBR E3 ubiquitin ligase HOIP. J. Am. Chem. Soc. *141*, 2703–2712. https://doi.org/10.1021/jacs.8b13193.

72. Strickson, S., Campbell, D.G., Emmerich, C.H., Knebel, A., Plater, L., Ritorto, M.S., Shpiro, N., and Cohen, P. (2013). The anti-inflammatory drug BAY 11-7082 suppresses the MyD88-dependent signalling network by targeting the ubiquitin system. Biochem. J. *451*, 427–437. https://doi.org/10.1042/BJ20121651.

73. Sakamoto, H., Egashira, S., Saito, N., Kirisako, T., Miller, S., Sasaki, Y., Matsumoto, T., Shimonishi, M., Komatsu, T., Terai, T., et al. (2015). Gliotoxin suppresses NF-κB activation by selectively inhibiting linear ubiquitin chain assembly complex (LUBAC). ACS Chem. Biol. *10*, 675–681. https://doi.org/10.1021/cb500653y.

74. Blessinger, S.A., Tran, J.Q., Jackman, R.P., Gilfanova, R., Rittenhouse, J., Gutierrez, A.G., Heitman, J.W., Hazegh, K., Kanias, T., and Muench, M.O. (2020). Immunodeficient mice are better for modeling the transfusion of human blood components than wild-type mice. PLoS One *15*, e0237106. https://doi.org/10.1371/journal.pone.0237106.

75. Li, T., Fu, J., Zeng, Z., Cohen, D., Li, J., Chen, Q., et al. (2020). TIMER2.0 for analysis of tumor-infiltrating immune cells. Nucleic Acids Res *48*, W509–W514. https://doi.org/10.1093/nar/gkaa407.

76. Li, W., Xu, H., Xiao, T., Cong, L., Love, M.I., Zhang, F., Irizarry, R.A., Liu, J.S., Brown, M., and Liu, X.S. (2014). MAGeCK enables robust identification of essential genes from genome-scale CRISPR/Cas9 knockout screens. Genome Biol. *15*, 554. https://doi.org/10.1186/s13059-014-0554-4.

77. Wang, B., Wang, M., Zhang, W., Xiao, T., Chen, C.H., Wu, A., Wu, F., Traugh, N., Wang, X., Li, Z., et al. (2019). Integrative analysis of pooled CRISPR genetic screens using MAGeCKFlute. Nat. Protoc. *14*, 756–780. https://doi.org/10.1038/s41596-018-0113-7.

78. Love, M.I., Huber, W., and Anders, S. (2014). Moderated estimation of fold change and dispersion for RNA-seq data with DESeq2. Genome Biol. *15*, 550. https://doi.org/10.1186/s13059-014-0550-8.

79. Yu, G., Wang, L.G., Han, Y., and He, Q.Y. (2012). clusterProfiler: an R package for comparing biological themes among gene clusters. OMICS *16*, 284–287. https://doi.org/10.1089/omi.2011.0118.

80. Wu, T., Hu, E., Xu, S., Chen, M., Guo, P., Dai, Z., Feng, T., Zhou, L., Tang, W., Zhan, L., et al. (2021). clusterProfiler 4.0: a universal enrichment tool for interpreting omics data. Innovation *2*, 100141. https://doi.org/10.1016/j.xinn.2021.100141.

81. Colaprico, A., Silva, T.C., Olsen, C., Garofano, L., Cava, C., Garolini, D., et al. (2016). TCGAbiolinks: an R/Bioconductor package for integrative analysis of TCGA data. Nucleic Acids Res *44*, e71. https://doi.org/10.1093/nar/gkv1507.

82. Ooft, S.N., Weeber, F., Dijkstra, K.K., McLean, C.M., Kaing, S., van Werkhoven, E., Schipper, L., Hoes, L., Vis, D.J., van de Haar, J., et al. (2019). Patient-derived organoids can predict response to chemotherapy in metastatic colorectal cancer patients. Sci. Transl. Med. *11*, eaay2574. https://doi.org/10.1126/scitranslmed.aay2574.

83. Dijkstra, K.K., Cattaneo, C.M., Weeber, F., Chalabi, M., van de Haar, J., Fanchi, L.F., Slagter, M., van der Velden, D.L., Kaing, S., Kelderman, S., et al. (2018). Generation of tumor-reactive T cells by Co-culture of peripheral blood lymphocytes and tumor organoids. Cell *174*, 1586–1598.e12. https://doi.org/10.1016/j.cell.2018.07.009.

84. Sato, T., Stange, D.E., Ferrante, M., Vries, R.G., Van Es, J.H., Van den Brink, S., Van Houdt, W.J., Pronk, A., Van Gorp, J., Siersema, P.D., and Clevers, H. (2011). Long-term expansion of epithelial organoids from human colon, adenoma, adenocarcinoma, and Barrett's epithelium. Gastroenterology *141*, 1762–1772. https://doi.org/10.1053/j.gastro.2011.07.050.

85. Ooft, S.N., Weeber, F., Schipper, L., Dijkstra, K.K., McLean, C.M., Kaing, S., van de Haar, J., Prevoo, W., van Werkhoven, E., Snaebjornsson, P., et al. (2021). Prospective experimental treatment of colorectal cancer patients based on organoid drug responses. ESMO Open *6*, 100103. https://doi.org/10.1016/j.esmoop.2021.100103.

86. Kong, X., Kuilman, T., Shahrabi, A., Boshuizen, J., Kemper, K., Song, J.Y., Niessen, H.W.M., Rozeman, E.A., Geukes Foppen, M.H., Blank, C.U., and

Peeper, D.S. (2017). Cancer drug addiction is relayed by an ERK2-dependent phenotype switch. Nature *550*, 270–274. https://doi.org/10.1038/nature24037.

87. Dobin, A., Davis, C.A., Schlesinger, F., Drenkow, J., Zaleski, C., Jha, S., Batut, P., Chaisson, M., and Gingeras, T.R. (2013). STAR: ultrafast universal RNA-seq aligner. Bioinformatics *29*, 15–21. https://doi.org/10.1093/bioinformatics/bts635.

88. Anders, S., Pyl, P.T., and Huber, W. (2015). HTSeq–a Python framework to work with high-throughput sequencing data. Bioinformatics *31*, 166–169. https://doi.org/10.1093/bioinformatics/btu638.

89. Subramanian, A., Tamayo, P., Mootha, V.K., Mukherjee, S., Ebert, B.L., Gillette, M.A., Paulovich, A., Pomeroy, S.L., Golub, T.R., Lander, E.S., and Mesirov, J.P. (2005). Gene set enrichment analysis: a knowledge-based approach for interpreting genome-wide expression profiles. Proc. Natl. Acad. Sci. U S A *102*, 15545–15550. https://doi.org/10.1073/pnas.0506580102.

90. Bankhead, P., Loughrey, M.B., Fernandez, J.A., Dombrowski, Y., McArt, D.G., Dunne, P.D., McQuaid, S., Gray, R.T., Murray, L.J., Coleman, H.G., et al. (2017). QuPath: open source software for digital pathology image analysis. Sci. Rep. *7*, 16878. https://doi.org/10.1038/s41598-017-17204-5.

STAR★METHODS

KEY RESOURCES TABLE

REAGENT or RESOURCE	SOURCE	IDENTIFIER
Antibodies		
RNF31 (recognizing human and mouse species)	R&D Systems	MAB8039; RRID: NA
RNF31 (recognizing human species)	Boster biological technology	A04457-3; RRID: NA
SHARPIN	Cell Signaling Technology	12541; RRID: AB_2797949
Caspase 3	Cell Signaling Technology	9665; RRID: AB_2069872
Cleaved Caspase 3	Cell Signaling Technology	9664; RRID: AB_2070042
RIPK1	Cell Signaling Technology	3493; RRID: AB_2305314
TNFR1	Santa Cruz Biotechnology	sc-8436; RRID: AB_628377
GAPDH	Absea Biotechnology	1617002D09; RRID: NA
Actin	Sigma-Aldrich	A2547; RRID: AB_476701
CD3	eBioscience	16-0037-85; RRID: AB_468855
CD8	eBioscience	16-0289-85; RRID: AB_468927
α-mouse TCR β chain	BD Biosciences	553172; RRID: AB_394684
Neutralizing TNF antibody	Cell Signaling Technology	7321; RRID: AB_10925386
Isotype for Neutralizing antibodies	Cell Signaling Technology	3900; RRID: AB_1550038
CD8 - BB515; clone: RPA-T8	BD Biosciences	564526; RRID: AB_1727513
CD4 - PerCP-eF710; clone: SK3	eBioscience	6-0047-42; RRID: AB_1834401
CD25 - PE-Dazzle 594; clone: M-A251	BioLegend	356126; RRID: AB_2563562
CD127 - Brilliant Violet 650; clone: A019D5	BioLegend	351326; RRID: AB_2562095
FOXP3 – APC; clone: 236A1E7	eBioscience	77-5774-40; RRID: AB_469980
Bacterial and virus strains		
E. coli strain: XL10-Gold Ultracompetent Cells	Internal stock	NA
1D3 virus	Internal stock	NA
Chemicals, peptides, and recombinant proteins		
LIVE/DEAD™ Fixable Near-IR Dead Cell Stain Kit	Themo Fisher	
CellTrace CFSE	Themo Fisher	C34554
CellTrace Violet (CTV)	Themo Fisher	C34557
Caspase-3/7 dye	Essen Bioscience	4440
Human recombinant TNF	Peprotech	300–01A
Murine recombinant TNF	ImmunoTools	12343010
Matrigel	Corning	356230
Retronectin	Takara	T100B
IL-2	Slotervaart Hospital	Proleukin
IL-7	ImmunoTools	11340075
IL-15	ImmunoTools	11340155
Crystal Violet	Sigma	V5265
Biotin-TNF	R&D Systems	BT210
Pierce™ Protein G Magnetic Beads	Themo Fisher	88848
Critical commercial assays		
Human TNF Flex Set Cytometric Bead Array (CBA)	BD Biosciences	558273
Human IFN-γ Flex Set Cytometric Bead Array (CBA)	BD Biosciences	558269
Dynabeads™ CD8 Positive Isolation Kit	Themo Fisher	11333D
STR profiling kit	Promega	B9510
Bradford Protein Assay	Bio-Rad	5000006
SuperSignal West Dura Extended Duration Substrate	Themo Fisher	34075

(*Continued on next page*)

Continued

REAGENT or RESOURCE	SOURCE	IDENTIFIER
NEBNext High Fidelity 2x PCR Master Mix	New England Biolads	M0541L
CellTiter-Blue	Promega	G8080
NEB® Golden Gate Assembly Kit (*Bsm*BI-v2)	New England Biolads	E1602
CellTiter-Glo 3D Viability Assay	Promega	G9681
Deposited data		
RNA sequencing Data	This paper	GEO: GSE186396
CRISPR/CAS9-screen MAGeCK results	This paper	Table S1
TCGA (SKCM, COAD, BRCA, LUSC, LUAD, LIHC) RNA sequencing Data	TCGA	https://portal.gdc.cancer.gov/
Pan-cancer analysis of whole genome (ICGC/TCGA, Nature 2020)	ICGC/TCGA	http://dcc.icgc.org/pcawg/
Proteomics	This paper	ProteomeXchange: PXD029489
Raw imaging data (Crystal violent staining images, Incucyte images, WB)	This paper; Mendeley Data	https://doi.org/10.17632/f52y9zkpzm.1
Raw quantification data (Crystal violent staining, FACS)	This paper; Mendeley Data	https://doi.org/10.17632/f52y9zkpzm.1
Experimental models: Cell lines		
HEK293T	Internal stock	RRID: CVCL_0063
D10 (Endogenous HLA-A2, Endogenous MART-1)	Internal stock	NA
BLM (Exogenous HLA-A2, Exogenous MART-1)	Internal stock	RRID: CVCL_7035
SW480 (Exogenous HLA-A2, Exogenous MART-1)	Internal stock	RRID: CVCL_0546
MCF7 (Exogenous HLA-A2, Exogenous MART-1)	Internal stock	RRID: CVCL_0031
B16F10 (Endogenous H2-Kb, Exogenous OVA)	Internal stock	RRID: CVCL_0159
LL/2 (Endogenous H2-Kb, Exogenous OVA)	Internal stock	RRID: CVCL_4358
MC38	Internal stock	RRID: CVCL_B288
CT26	Internal stock	RRID: CVCL_7256
Experimental models: Organisms/strains		
NSG-β2M^{null} mice	The Jackson Laboratory	010636; RRID: IMSR_JAX:010636
C57BL/6J mice	Janvier	C57BL/6JRj
Oligonucleotides		
the List of Oligonucleotide Sequences for Sequencing and sgRNAs	This Paper	Table S2
Recombinant DNA		
lentiCRISPR-v2	Addgene	RRID: Addgene_83480/ RRID: Addgene_52961
psPAX	Addgene	RRID: Addgene_12260
pMD2.G	Addgene	RRID: Addgene_12259
lentiCas9-Blast	Addgene	RRID: Addgene_52962
GeCKO whole-genome knockout library	Addgene	1000000049
Software and algorithms		
TIMER2.0	Li, T. et al., 2020[75]	http://timer.cistrome.org/
Proteome Discoverer 2.2	Thermo Scientific	OPTON-30795
GraphPad Prism 9 (v9.0.0)	Graphpad Software Inc.	https://www.graphpad.com/scientific-software/prism/
R (v4.1.1)	R	https://cran.r-project.org/
RStudio (v1.4.1106)	RStudio, PBC	https://www.rstudio.com/
ImageJ	ImageJ	https://imagej.nih.gov/ij/
MAGeCK algorithm (v0.5.9.4)	Li et al., 2014[76]	https://sourceforge.net/p/mageck/wiki/
MAGeCKFlute (v1.10.0)	Wang et al., 2019[77]	https://bioconductor.org/packages/release/bioc/html/MAGeCKFlute.html

(*Continued on next page*)

Continued

REAGENT or RESOURCE	SOURCE	IDENTIFIER
DESeq2 (version1.30.1)	Love et al., 2014[78]	https://bioconductor.org/packages/release/bioc/html/DESeq2.html
clusterProfiler (v4.1.4)	Wu et al., 2021;[79] Yu et al., 2012[80]	https://bioconductor.org/packages/release/bioc/html/clusterProfiler.html
TCGAbiolinks (v2.22.3)	Colaprico et al., 2016[81]	https://bioconductor.org/packages/release/bioc/html/TCGAbiolinks.html
cBioPortal		http://www.cbioportal.org/
FlowJo (v10)	FlowJo, LLC	https://www.flowjo.com/
Other		
NovaSeq 6000 System	illumina	https://www.illumina.com/systems/sequencing-platforms/novaseq.html

RESOURCE AVAILABILITY

Lead contact

Further information and requests for resources and reagents should be directed to and will be fulfilled by the Lead Contact Daniel S. Peeper (d.peeper@nki.nl).

Materials availability

The materials generated in this study did not generate new unique reagents.

Data and code availability

- CRISPR screens were analyzed using publicly available MAGeCK (v0.5.9.4, https://sourceforge.net/p/mageck/wiki/Home/). The MAGeCK results of genome-wide screen in D10 Melanoma challenged with $CD8^+$ T or NK cells are shown in Table S1. The RNA-seq raw dataset generated here is available in the SRA repository and can be accessed using GEO accession numbers GSE186396 (https://www.ncbi.nlm.nih.gov/geo/query/acc.cgi?acc=GSE186396). The proteomics data was submitted to ProteomeXchange under the identification number ProteomeXchange: PXD029489.
- All the R scripts used in this study are available upon request and without restriction to the Lead contact (d.peeper@nki.nl).
- Any additional information required to reanalyze the data reported in this work paper is available from the Lead contact upon request.

EXPERIMENTAL MODEL AND SUBJECT DETAILS

Human primary $CD8^+$ T cells and NK cells

Human peripheral blood mononuclear cells (PBMCs) were isolated from fresh healthy donor buffy coats (Sanquin, Amsterdam, the Netherlands) by density gradient centrifugation with Ficoll-Paque PLUS density gradient media (17144003, GE healthcare). Fresh healthy donor buffy coats (B2825R00) were obtained from Sanquin (Amsterdam, the Netherlands). The clinical information of healthy donors was recorded by Sanquin Blood Supply Headquarters, the Netherlands. $CD8^+$ T cells were further purified from PBMC fractions using CD8 Dynabeads (Thermo Fisher Scientific) following the product manual. Isolated CD8 cells were activated for 48 h on a 24-well plate that was pre-coated overnight with CD3 and CD28 antibodies (eBioscience, 5 μg per well) at 2×10^6 per well. 2×10^6 activated CD8 T cells were spinfected with 1:1 MART-1 TCR retrovirus on a Retronectin-coated (Takara, 25 μg per well) non-tissue culture treated 24-well plate for 2 h at 2000 g. After 24 h infection, MART-1 T cells were harvested and cultured for 7 days, and MART-1 TCR expression was confirmed by flow cytometry (BD PharMingen, α-mouse TCR β chain). CD8 T cells were initially maintained in RPMI (GIBCO) containing 10% human serum (One Lamda), 100 U/mL penicillin, 100 μg/mL streptomycin, 100 U/mL IL-2 (Proleukin, Novartis), 10 ng/mL IL-7 (ImmunoTools) and 10 ng/mL IL-15 (ImmunoTools). After retroviral transduction, T cells were maintained in RPMI containing 10% fetal bovine serum and 100 U/mL IL-2. For primary NK cell isolation and expansion, PBMCs were co-cultured with gamma-irradiated Jurkat cells in RPMI-1640 medium with IL-2 (100 U/mL) for 7 days and subsequently subjected to a Dynabeads™ Untouched™ Human NK Cells Kit (11349D, ThermoFisher). Isolated NK cells were cultured in RPMI-1640 medium with 9% FBS and IL-2 (100 U/mL). The study procedures were approved by the local Institutional Review Board committee.

Colorectal organoids

Three patient-derived organoid (PDO) lines (ITO-066, ITO-079 and ITO-111) established from colorectal tumors were derived from the personal biobank of Voest group, or their prior studies.[82,83] The clinical information about patient tumors were recorded in study

NL48824.031.14 in the Netherlands Cancer Institute. Patient organoids are available for sharing as defined in the signed informed consent (study NL48824.031.14), and as approved by the Medical Ethical Committee of the Netherlands Cancer Institute – Antoni van Leeuwenhoek hospital.[83] The PDOs used were cultured and expanded according to the standard described protocol.[84,85] PDOs were expanded and cultured from working biobanks, typically passage four or lower. Cultures were checked for mycoplasma contamination every month using the MycoAlert Mycoplasma Detection Kit (Lonza). As part of quality control, PDOs were authenticated using a TaqMan-based SNP array targeting 26 single-nucleotide polymorphisms (SNPs) (Hartwig Medical Foundation).

Cell lines

Human melanoma cell lines (D10, BLM, and A101D), breast cancer cells (MCF-7), colorectal cells (SW480), embryonic kidney cells HEK293T, and murine melanoma cell line B16F10, colorectal cell lines (MC38 and CT26), and murine Lewis lung carcinoma cell line LL/2 were all from Peeper lab cell stocks. B16F10-OVA and LL/2-OVA cell lines were generated by transduction with OVA cDNA, expressing the ovalbumin antigen. For co-culturing with MART-1 $CD8^+$ T cells, human cancer cell lines that do not have endogenous HLA-A*02:01 or MART-1 expression were lentivirally transduced with the corresponding cDNA. Human natural killer cell line KHYG-1 was purchased from Leibniz Institute DSMZ (Brunswick, Germany) and was cultured with RPMI-1640 with 9%FBS and IL2 (100 U/mL). All cells were cultured in DMEM supplemented with 9% fetal bovine serum (Sigma) plus 100 U/mL penicillin and 0.1 mg/mL streptomycin (Gibco) except otherwise specified. All cell lines were authenticated by STR profiling and routinely tested for mycoplasma contamination.

Animal studies

Animal work procedures were approved by the animal experimental committee (Instantie voor Dierenwelzijn) of the institute according to Dutch law and performed in accordance with ethical and procedural guidelines established by the NKI and Dutch legislation. The *in vivo* experiments were performed with B16F10-OVA, MC38 cells and D10 infected with lentivirus encoding sgRNAs. 5×10^5 B16F10-OVA or MC38 cells and 1×10^6 D10 cells were injected subcutaneously into the right flanks of NSG-B2m (Jax, bred at NKI) or C57/BL6 mice (Janvier). Male mice were used at an age of 8–12 weeks. All animals are housed in disposable cages in the laboratory animal center (LAC) of the NKI, minimizing the risk of cross-infection, improving ergonomics and obviating the need for a robotics infrastructure for cage-washing. The mice were kept under specific pathogen free (SPF) conditions. Tumor size was monitored three times per week with calipers by measuring tumor length (L) and width (W), and calculating volume through the use of the formula $LW^2/2$. All experiments ended for individual mice either when the total tumor volume exceeded 500, 1000 or 1400 mm^3, when the tumor showed ulceration, in case of serious clinical illness, when the tumor growth blocked the movement of the mouse, or when tumor growth assessment had been completed.

METHOD DETAILS

Genome-wide CRISPR-cas9 knockout (GeCKO) screen

Human D10 melanoma cells (600 million cells) were lentivirally transduced with the GeCKO libraries (A and B) with a MOI of 0.3. Two days after infection, cells were selected with puromycin (2 μg/mL) for 3 days and T0 samples were collected. One week later, cells were split into three pools; one arm was subjected to a co-culture with MART-1 $CD8^+$ T cells (T cell:tumor ratio at 1:8), another arm with KHYG-1 cells (NK: tumor ratio at 1:2), while the third arm was left untreated. After 2 days of co-culture, cells were washed twice with PBS and cultured for another 4 days. The surviving cells were harvested and genomic DNA was isolated using a Blood and Cell Culture MAXI kit (13362, Qiagen). sgRNA sequences were recovered by PCR using NEBNext High-Fidelity 2x PCR Master Mix (M0541L, New England BioLabs) with the following primers:

GeCKO forward:

5′-AATGATACGGCGACCACCGAGATCTACACTCTTTCCCTACACGACGCTCTTCCGATCTNNNNNNGGCTTTATATATCTTGTG GAAAGGACGAAACACC- 3′

GeCKO reverse:

5′-CAAGCAGAAGACGGCATACGAGATCCGACTCGGTGCCATTTTTCAA-3′

The stretch of six N nucleotides indicates a unique barcode for the identification of each sample. The amplified PCR products were purified, pooled equimolarly and subjected to deep sequencing (HiSeq 2500 System, Illumina). Obtained sequence reads were aligned to the Gecko A and B libraries and counts per sgRNA were generated, where reads containing mismatches in common and sgRNA sequences were excluded for analysis. Enrichment and depletion at the sgRNA and gene level were determined using the MAGeCK algorithm (v0.5.9.4).[76] Enrichment and depletion of genes in the $CD8^+$ T cell or NK cell samples were determined relative to untreated samples. The results were analyzed using MAGeCKFlute package (v1.10.0)[77] in R. The MAGeCK RRA scores were used to assess depleted genes and enriched genes for both $CD8^+$ T cell screen and NK cell screen. -Log10 transformed RRA score at three was used as cutoff.

Immunoblotting

Immunoblotting was performed as previously described.[86] The following antibodies were used: RNF31 (MAB8039) (recognizing human and mouse species) from R&D Systems; RNF31(A04457-3) (recognizing human species) from Boster biological technology; SHARPIN (12541), Caspase 3 (9665), Cleaved Caspase 3 (9664), RIPK1 (3493) from Cell Signaling Technology, TNFR1 (sc-8436) from Santa Cruz Biotechnology; GAPDH (1617002D09) from Absea Biotechnology (Beijing, China); Actin (A2547) from Sigma-Aldrich.

Compound and recombinant proteins

RNF31 inhibitor HOIPIN-8 (2972) was synthesized by Axon Medchem (Groningen, the Netherlands). Recombinant human IL-2 (Proleukin) was obtained from Slotervaart hospital. Recombinant human TNF (300–01A) was obtained from Peprotech, recombinant human IL-7 (11340075), human IL-15 (11340155), mouse TNF (12345010), mouse IL-2 (12340020), mouse IL-7 (12340073) and mouse IL-15 (12340153) from Immunotools.

sgRNA construction and lentivirus production

Cloning of the sgRNA constructs and production of lentivirus for sgRNAs expression were performed as previously described.[86] Double knockouts were generated by using both a puromycin-selectable and blasticidin-selectable variant of lentiCRISPR-v2 for each sgRNA. To establish clonal knockout cell lines, tumor cells were transfected with lentiCRISPR-v2 and clones were generated by limiting dilution or soft-agar colonies were picked. To generate B16F10-OVA B2M-deficient cell lines, tumor cells were transfected with lentiCRISPR-v2, selected with puromycin and FACSorted three times based on lack of expression of H-2kb after treatment with IFNγ. The sequences of sgRNAs were in Table S2.

Competition assay

Cells containing sgRNAs of interest were labeled either with CellTrace CFSE (CFSE, C34554, ThermoFisher) or CellTrace Violet (CTV, C34557, ThermoFisher), mixed at 1:1 ratio and plated in 6-well plates (1×10^6 cells per well for D10, 2×10^5 cells for BLM) in triplicate. Labeled cells were challenged with either MART-1 $CD8^+$ T cells (E:T of 1:8 for D10, 1:2 for BLM), primary NK cells (1:3 for both D10 and BLM), KHYG-1 (1:2 for D10, 4:1 for BLM) or untreated for 2 days. Cells were then washed with PBS twice and cultured for another 3 days before analysis by FACS.

Cytokine measurements

The concentration of cytokines (TNF and IFNγ) in the co-culture system were measured using the Human TNF and IFNγ Flex CBA kit (BD Biosciences), following manufacturer's instructions. The isolated medium was harvested after 48 h co-culture and incubated with CBA beads and analyzed by FACS.

Flow cytometry

Cells were stained with antibodies targeting surface or intracellular molecules of interest according to manufacturer's instructions and analyzed on a Fortessa flow cytometer (BD Bioscience). Antibodies against mouse TCR β:Hamster-PE (1:200 dilution, Biolegend, H57-597), human CD8:PacificBlue (1:50 dilution, BD, RPA-T8), human CD8:BB515 (1:100 dilution, BD, RPA-T8), human CD4:PerCP-eF710 (1:100 dilution, eBioscience, SK3), human CD25:PE-Dazzle 594 (1:100 dilution, Biolegend, M-A251), human CD127:Brilliant Violet 650 (1:100 dilution, Biolegend, A019D5) and human FoxP3:APC (1:100 dilution, eBioscience, 236A1E7) were used. The dyes Life/Dead (1:1000 dilution, Themo Fisher) and CTV (1:1000 dilution, Themo Fisher) were used to stain cells.

In vitro cytotoxicity assays

Tumor cells were seeded into 12-well or 24-well culture plates (Greiner). For 12-well plates, per well 2×10^5 SW480 cells, 1×10^5 MCF7 cells, 1×10^5 BLM, 1.5×10^5 D10, 1.5×10^5 B16F10-OVA were seeded. For 24-well plates, per well 1×10^5 SW480 cells, 0.6×10^5 MCF7 cells, 0.5×10^5 BLM cells, 0.8×10^5 D10 cells, 0.8×10^5 B16F10-OVA, LL/2-OVA, MC38 and CT26 cells were seeded. $CD8^+$ T cells or NK cells were admixed in serial dilutions (2-fold). Where indicated, 10 μM or 20 μM of HOIPIN-8 in DMSO was added to co-cultures. For NK cell co-cultures, 100 U/mL IL-2 was supplemented. After 24 h, $CD8^+$ T or NK cells were washed off. After a further 3–5 days, cells were fixed and stained for 1 h using a solution containing 0.1% crystal violet (Sigma) and 50% methanol (Honeywell). When indicated, a neutralizing TNF antibody or isotype control (Cell Signaling Technology) was added at a concentration of 1 μg/mL. For quantification, crystal violet was solubilized in 10% acetic acid (Sigma). Absorbance of this solution was measured on an Infinite 200 Pro spectrophotometer (Tecan) at 595nm. For Incucyte (Incucyte Zoom, Essen Bioscience) experiments, 5×10^3 tumor cells were seeded per well in 96-well culture plates (Greiner). $CD8^+$ T or NK cells were admixed in indicated ratios and a Caspase-3/7 GFP dye (Essen Bioscience) was added. Growth of these co-cultures was followed for 72 h. When indicated, instead of CD8 T or NK cells, 100 ng/mL recombinant TNF (Peprotech) at indicated concentrations was added. To perform a dose-response with TNF, 100 ng/mL of TNF was added to melanoma cells as the highest dilution and serially diluted.

Organoid culture and TNF sensitivity assay

Three patient derived organoid (PDO) lines were established from colorectal tumors. The PDOs used were cultured and expanded according to the previously described protocol.[84] For western blot analysis the organoids were pretreated with HOIPIN8 for 20 h in a

concentration of 5, 10, 20 μM, or DMSO as a negative control in regular colorectal cancer organoid medium.[84] After the pretreatment, TNF was added in a concentration of 100 ng/mL, for two or 6 h. The extracellular matrix (basement membrane extract, manufacturer) was removed by incubating with 2 mg/mL type-II dispase (D4693, Sigma-Aldrich) for 15 min at 37°C. After removal of the matrix, the cells were washed and lysed for Western Blot analysis.

The TNF sensitivity assays were performed in the same way as previously described.[82] Regular CRC organoid culture medium was supplied with hTNF in a concentration of 1 ng/mL, 10 ng/mL, 50 ng/mL and 100 ng/mL, with or without addition of 10 μM HOIPIN8. The readout was performed by assessment of cell viability with the CellTiter-Glo 3D Viability Assay (G9681, Promega), according to manufacturer instructions using an Infinite 200 Pro plate reader (Tecan Life Sciences). The raw data was normalized over the untreated condition, after subtraction of the background signal, and then plotted in GraphPad Prism (version 8.0.0).

B16F10-OVA mixing experiments

B16F10-OVA cells were mixed at different ratios with either B16F10 parental cells or B16F10-OVA B2M KO cells (1×10^4 cells per well in 12-well plates). Different ratios of OT-1 T cells were added subsequently and supplemented with HOIPIN-8 or vehicle. Co-cultures with OT-1 T cells were for 3 days and the plates were fixed with formaldehyde and stained with crystal violet solution.

TNF co-immunoprecipitation and mass spectrometry

1×10^7 BLM cells (sgCtrl or sgRNF31) were cultured with the addition of HOIPIN-8 (20 μM) or vehicle for 24 h before treatment with 100 ng/mL biotinylated TNF (BT210–010, R&D Systems) or unlabeled TNF (Peprotech) for 10 min. Cells were then collected and lysed in IP lysis buffer (30 mM Tris-HCl pH 7.4, 120 mM NaCl, 2 mM EDTA, 2 mM KCl, 1% Triton X-100 and supplemented with protease inhibitor cocktail (04693159001, Roche)). TNF receptor complexes were then precipitated by using streptavidin-coated magnetic beads (88816, Thermo Fisher Scientific) for 1 h at 4°C and subsequently analyzed by mass spectrometry. Purified protein complexes were eluted from magnetic beads using a 5% SDS solution and were digested using S-TRAP microfilters (ProtiFi) according to the manufacturer's protocol. Briefly, eluted samples were reduced and alkylated using DTT (20 mM, 10 min, 95°C) and IAA (40 mM, 30 min). Next, samples were acidified and proteins were precipitated using a methanol TEAB buffer before loading on the S-TRAP column. Trapped proteins were washed 4 times with the methanol TEAB buffer and then digested for 1 h at 47°C using 1 μg Trypsin (Promega). Digested peptides were eluted and dried in a vacuum centrifuge before LC-MS analysis.

LC-MS/MS analysis and data processing

Samples were analyzed by reversed phase nLC-MS/MS using an Agilent 1290 HPLC coupled to an Orbitrap Q Exactive HF-X mass spectrometer (Thermo Scientific). Digested peptides were separated using a 50 cm reversed phase column packed in-house (Agilent Poroshell EC-C18, 2.7 μm, 50 cm × 75 μm) and eluted at a flow rate of 200 nL/min using a linear gradient with buffer A (0.1% FA) and buffer B (80% ACN, 0.1% FA) ranging from 10–36% B over 155 min, followed by a column wash and re-equilibration step. The total data acquisition time was 175 min. MS data was acquired using a DDA method with the following MS1 scan parameters: 60,000 resolution, AGC target equal to 3E6, maximum injection time of 20 ms, scan range of 375–1600 *m/z*, acquired in profile mode. The MS2 method was set at 30,000 resolution, with an AGC target of 1E5, a maximum injection time of 50 ms, and an isolation window of 1.4 *m/z*. Scans were acquired used a mass range of 200–2000 and an NCE of 27. The top 15 precursors ions were selected for with a dynamic exclusion time set to 24 s, and a precursor charge selection filter for ion possessing +2 to +5 charges. Raw files were processed using MaxQuant (version 1.6.7). MS/MS fragment spectra were searched against a human database (UniProt, year 2019) and common contaminants database. Default analysis settings were applied in MaxQuant with the following search modifications: methionine oxidation, protein N-term acetylation, and phosphorylation of serine, threonine, and tyrosine were set as variable modifications. Cysteine carbamidomethylation was set as a fixed modification. Trypsin digestion was selected with a maximum of two missed cleavages. A false discovery rate (FDR) of 1% was applied at the protein, peptide, and modification level. A site localization probability of at least 0.75 was used as thresholds for the localization of phosphorylated residues (class I phosphosites). Protein abundances were calculated using label free quantification with default settings applied. Database search results were further processed in Perseus (version 1.6.12) for statistical analysis.

RNA isolation and mRNA expression analysis

1×10^5 BLM sgCtl or sgRNF31 cells were pretreated with vehicle (DMSO) or HOIPIN-8 (10 μM) for 16 h, followed by TNF stimulation (100 ng/mL) for 0 or 6 h. Two replicates for each sample were performed. Cell culture medium was removed and washed twice with ice-cold PBS. Cells were then lysed by adding 600 μL of buffer RLT (Qiagen, 79216) and their total RNA extracted using a RNeasy mini kit (Qiagen, 74106) according to the manufacturer's instructions. PolyA + stranded RNA Libraries were generated using the TruSeq Stranded mRNA sample preparation kit (Illumina) by NKI Genomics Core Facility. Briefly, total RNA was fragmented and randomly primed. Strand-specific first strand cDNA was reverse transcribed using Super-Script II Reverse Transcriptase (Invitrogen) with the addition of actinomycin D. The second cDNA strand was synthesized using polymerase I and RNaseH with dUTP in place of dTTP. The generated cDNA fragments were then 'A-tailed' at the 3′ end, adapter dimerization, ligated and amplified by PCR. The libraries were validated on a 2100 Bioanalyzer using a 7500 chip (Agilent) and pooled. Samples were sequenced on a NovaSeq 6000 instrument (Illumina) using a 51-bp paired end run. FASTQ files were mapped to the human reference genome hg38 using STAR

(version 2.7)[87] with default settings. Genes reads counted using HTSeq2 (version 0.11.1)[88]. Count data were analyzed in RStudio (version 1.4.1106) with DESeq2 (version1.30.1).[78]

RNA sequencing count data were normalized using rlog-transformation as implemented in DESeq2. Differentially expressed genes (DE-Gs) were calculated using DESeq2, then p.adj <0.05 and fold change >1.5 were used as cutoffs. RNF31 inhibition signature comprised common significant DE-Gs upregulated by sgRNF31 and HOIPIN-8 after TNF stimulation. Gene set enrichment analysis (GSEA) was performed in R using clusterProfiler package (version 4.1.4)[79,80] with pre-ranked log2 fold change of gene expression as a metric, and using the C2-CP sub-collection from MSigDB.[89] GSEA plots were redrawn using the gseaplot2 function from enrichplot package (https://github.com/YuLab-SMU/enrichplot).

Clinical data analysis

For the analysis in Figure 7A, TIMER2.0[75] (http://timer.cistrome.org/) was used to query the gene expression profile among different TCGA cancer subtypes, and the downloaded files were replotted. Distributions of gene expression levels are displayed using boxplots. The statistical significance computed by the Wilcoxon test is annotated by the number of stars (*: p value < 0.05; **: p value <0.01; ***: p value <0.001). For indicated TCGA cancer subtypes, the raw count and clinical data were downloaded from TCGA by using TCGAbiolinks[81] (v2.22.3). The raw count was firstly normalized to TPM (transcripts per million) based on GENCODE v22 reference. The expression of LUBAC complex was calculated using the average expression of RNF31, SHARPIN and RBCK1. The log2(TMP + 1) expression was plotted for primary tumor and normal tissues. The statistical significance computed by the Wilcoxon test is annotated by the number of stars (*: p value < 0.05; **: p value <0.01; ***: p value <0.001). Expression of RNF31 at different disease stages were presented as log2(TPM + 1) and analyzed by a Kruskal-Wallis test (*: p value < 0.05; **: p value <0.01; ***: p value <0.001). We removed the metastatic and normal tissue samples in the BRCA cohort and removed normal tissue samples in SKCM cohort to conduct survival analysis. The Kaplan-Meier survival curve was analyzed using survival (v3.2-11) and plot using survminer (v0.4.9). TNF expression and RNF31 expression are grouped by quartile cutoff levels. p value was computed by Log-Rank test.

IHC and quantification

The collection and use of mouse tumor tissue was approved by the animal experimental committee of the institute and performed according to Dutch law. CD8 (14–0808, eBioscience) and NKp46 (AF2225, R&D Systems) stainings were performed using the Ventana autostainer using the standard protocol, using counterstain with haematoxylin, and manually analyzed and scored blindly by a certified pathologist.

Positive cell detection of $NKp46^+$ cells was performed by a pathologist (S.K.) who was blinded to the RNF31 expression status of the two experimental groups. Within each tumor, positive cells were manually counted in three randomly picked circular areas of 0.8 mm^2 within viable tumor tissue. Necrotic areas contained non-specific IHC signal associated with cellular debris and were excluded from the analysis. The slides were scanned in a Panoramic 1000 system (3DHISTECH) and viewed in SlideScore (https://www.slidescore.com/). Positive cell detection of $CD8^+$ cells was performed in Qupath.[90] The RGB signal was first split into a two separate stains with the stain vector [0.65, 0.70, 0.29] for hematoxylin and [0.27, 0.57, 0.78] for DAB. The positive cell detection plugin was set to detect cells where the DAB optical density in the whole cell was higher than 0.15. The script for automation of this workflow is available upon request.

QUANTIFICATION AND STATISTICAL ANALYSIS

Statistics

To compare two means, a two-tailed Student's t test was used. To compare multiple groups of data to one control condition, we performed a one-way ANOVA, followed by a Dunnett's test to correct for multiple comparisons. For two factors with multiple groups, selected comparisons were made by two-way ANOVA followed Sidak's multiple comparisons test. *In vivo* data were compared by a multiple unpaired two-sided Student's t-test when data were normally distributed. When data were not normally distributed, Shapiro-Wilk test was used. Survival analyses were performed by Log Rank Mantel-Cox test, followed by Holm-Sidak multiple testing correction. Exceptions to these approaches are listed in the corresponding figure legends. Analyses were performed by Prism 9 (Graphpad Software Inc., version 9.0.0) or in R. Unless otherwise indicated, a p value of lower than 0.05 was regarded as being statistically significant. ***, $p < 0.001$, **, $p < 0.01$, *, $p < 0.05$.